Czech Technical University in Prague
Faculty of Electrical Engineering
Department of Cybernetics

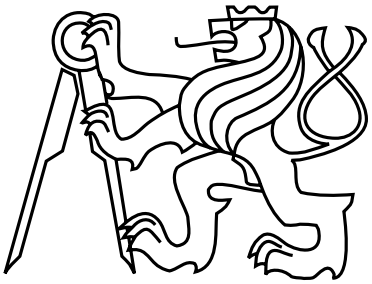

Bachelor's Thesis

Modeling of Launch Vehicle during the Lift-off Phase in Atmosphere

Matyáš Lustig

Supervisor: doc. Ing. Martin Hromčík, Ph.D.

Study Programme: Cybernetics and Robotics
Field of Study: Robotics
Bachelor's degree

May 18, 2017

Czech Technical University in Prague
Faculty of Electrical Engineering

Department of Cybernetics

BACHELOR PROJECT ASSIGNMENT

Student: Matyáš L u s t i g

Study programme: Cybernetics and Robotics

Specialisation: Robotics

Title of Bachelor Project: Modeling of Launch Vehicle during the Lift-off Phase in Atmosphere

Guidelines:

The objective of this thesis is to provide a platform for model-based simulation and control laws validation of launch vehicles. The emphasis is put on the lift-off phase of the rocket flight which is analysed using a mathematical flight dynamics model. An expected result of the Bachelor thesis are also simulation and practical experiment illustrating advanced physical phenomena of a real rocket flight.

1. Get familiar with the principals of rocket engineering and rocket science.
2. Develop a flight mechanics model of a launch vehicle during the lift-off phase of a flight through the atmosphere.
3. Create a dedicated simulation scheme in the MATLAB/Simulink environment.
4. Design, execute and document selected practical experiments, related either to flight identification and validation of the simulation model, or to flight testing of selected control algorithms.

The water-rocket developed within a FEL SGS project, with its on-board unit, may be used as the experimental platform.

Bibliography/Sources:

[1] Arthur E. Bryson, Jr. - Control of Spacecraft and Aircraft - 1994, Princeton, New Jersey, USA
[2] John H. Blakelock - Automatic Control of Aircraft and Missiles, 2nd edition - 1991, USA

Bachelor Project Supervisor: doc. Ing. Martin Hromčík, Ph.D.

Valid until: the end of the summer semester of academic year 2017/2018

L.S.

prof. Dr. Ing. Jan Kybic
Head of Department

prof. Ing. Pavel Ripka, CSc.
Dean

Prague, December 2, 2016

Acknowledgements

I would like to express my gratitude to my supervisor, doc. Ing. Martin Hromčík, Ph.D. for all the suggestions and advice he has offered me during the work on this thesis. I am grateful to my parents for their continuous encouragement and to Eva who read my first thesis.

Declaration

I declare that the presented work was developed independently and that I have listed all sources of information used within it in accordance with the methodical instructions for observing the ethical principles in the preparation of university theses.

In Prague on May 18, 2017 .....

Abstract

The objective of this thesis is to provide a platform for model based simulation and control laws validation of launch vehicles. The lift-off phase of the rocket flight is analyzed using a mathematical nonlinear dynamics model. Full set of six degrees of freedom equations of motion is developed with combination of auxiliary computations and necessary reference frames and transformations in between them. The mathematical model is employed by comprehensive MATLAB and Simulink simulation which can be easily adjusted for any type of launch vehicle or rocket. The simulation model has been validated and linearized for a further analysis. Water rocket practical experiment demonstrates the simulation platform capabilities.

Abstrakt

Práce pojednává o vývoji platformy pro počítačovou simulaci letu raketových nosičů, jež může být použita i pro návrh a validaci automatického řízení. Dynamický nelineární model sestávající z pohybových rovnic uvažujících šest stupňů volnosti rakety, podpůrných výpočtů a transformací mezi souřadnými systémy popisuje vzletovou fázi letu rakety v atmosféře. Na základě matematického modelu je v prostředí MATLAB a Simulink navržen model simulační. Výstupy simulační platformy jsou ověřeny a porovnány s očekávaným chováním raketového nosiče. Nelineární model je dále zlinearizován pro hlubší analýzu. Možnosti simulačního modelu demonstruje praktický experiment s vodní raketou, kdy jsou výsledky simulace srovnány s daty z reálného letu.

Contents

List of Figures

List of Tables

Chapter 1

Introduction

The ultimate task of a launch vehicle is to safely transport any kind of payload to an orbit around the Earth. Most of the missions are covering highly valuable satellites or deep space probes and some even serve for manned mission - to the Moon, to the ISS and maybe one day in not so far future to other planets. Thus, a great attention is being paid to carrier rockets reliability and development.

Aerospace along with military industry have always been the driving power of progress and innovation in many different fields in modern history. The fastest advancement took place during the Cold War renowned space race between the USA and the USSR resulting in landing a man on the Moon. However, we have never really stopped exploring our surroundings. Recently, several initiatives became rife trying to push boundaries of humanity further again. Elon Musk has revealed fearless plans for manned missions to Mars with SpaceX company which already successfully operates its highly innovative Falcon 9 rocket. Jeff Bezos with his company Blue Origin has set himself the task of opening up the space to broader public. And even the Czech Technical University is close to establishing a partnership with a company which specializes in small class launch vehicles manufacturing. Apparently, the aerospace industry is once again coming alive.

Design and manufacturing of rockets is a highly demanding and protracted process. Before you can even start, you have to penetrate the physical processes occurring during an atmospheric and space flight. This thesis is aiming to develop a mathematical model of launch vehicle's flight focusing on the lift-off phase in the Earth's atmosphere. We begin with defining various reference frames embracing the whole launch vehicle's environment. Kinematic and dynamic models of rocket flight are developed resulting in a set of equations of motion. Likewise, individual physical sub-models are utilized and described.

All together, the mathematical model serves as a basis for computer simulation development. Mighty software MATLAB is utilized with combination of Simulink to create an exact and interactive simulation of launch vehicle's flight. Basic flight laws may be verified and certain situations or maneuvers demonstrated. A practical experiment with water rocket model has been conducted at the CTU in the past and we will pick up its threads by validating our simulation model with flight data obtained during that occasion. Let's start the countdown!

Chapter 2

Goals

Based on the thesis' guidelines enclosed, several goals have been set. The following tasks have been laid out and the work will hopefully resolve all of them.

1. Get acquainted with the state of the art of rocket engineering and rocket science.
2. Develop a flight mechanics model of a launch vehicle during the lift-off phase of a flight through the Earth's atmosphere.
3. Create a simulation scheme in the MATLAB or Simulink environment and validate the simulation's results.
4. Linearize the nonlinear model and perform a basic sensitivity analysis.
5. Design, execute and document a practical experiment with the water rocket model. Calibrate the simulation model with respect to the obtained flight data.

Chapter 3

Mathematical Model

3.1 Reference Frames

Firstly, several frames of reference are introduced in order to describe the position and motion of the launch vehicle in space in accordance with *Zipfel* [1]. Reference frames are understood as right handed Cartesian coordinate systems specified by their orientation in space. Certain trade-off has to be made between the number of frames used by the model and the clarity of problem description. Following reference frames have been chosen because together they are capable of complete characterization of the launch vehicle's motion.

The use of more reference frames implies necessity to coordinate transformations between them. Appropriate transformation rotational matrices are presented for each two subsequent frames. Any more complex or inverse transformations can be built upon the individual ones.

3.1.1 Earth Centered Inertial Reference Frame

For any space travel in our solar system, the heliocentric frame represents the inertial frame of reference. However, for flights close to the surface or in the atmosphere, the Earth centered frame is sufficient. Origin of such coordinate system lies at the center of mass of the Earth. We use the J2000 system with basis vectors $\hat{i}, \hat{j}, \hat{k}$ given as follows. The vector $\hat{i}$ lies in the equatorial plane pointing towards the vernal equinox (intersection of ecliptic with the Earth's equator in spring) in J2000 epoch (1st January 2000, 12:00 Terrestrial time). The $\hat{k}$ vector is normal to the equatorial plane, coincides with the Earth's axis of rotation and points to the North pole. The remaining basis vector $\hat{j}$ lies in the equatorial plane and completes the right-handed Cartesian system. The frame may be referred to as the *inertial* one or by the abbreviation *ECI*.

3.1.2 Earth Centered Fixed Reference Frame

The origin of the Earth centered fixed frame also lies in the center of Earth. Let's describe it with another set of basis vectors $\hat{i}_e, \hat{j}_e$ and $\hat{k}_e$. First vector $\hat{i}_e$ is defined as pointing from the center of the Earth to the intersection of the Earth's prime Greenwich meridian with the equator. Vector $\hat{k}_e$ is aligned along the Earth's spin axis and thus coincides with the

ECI's basis vector $\hat{k}$. Vector $\hat{j}_e$ completes the right-handed Cartesian coordinate system. The frame may be referred to as an *Earth* or *ECF* one.

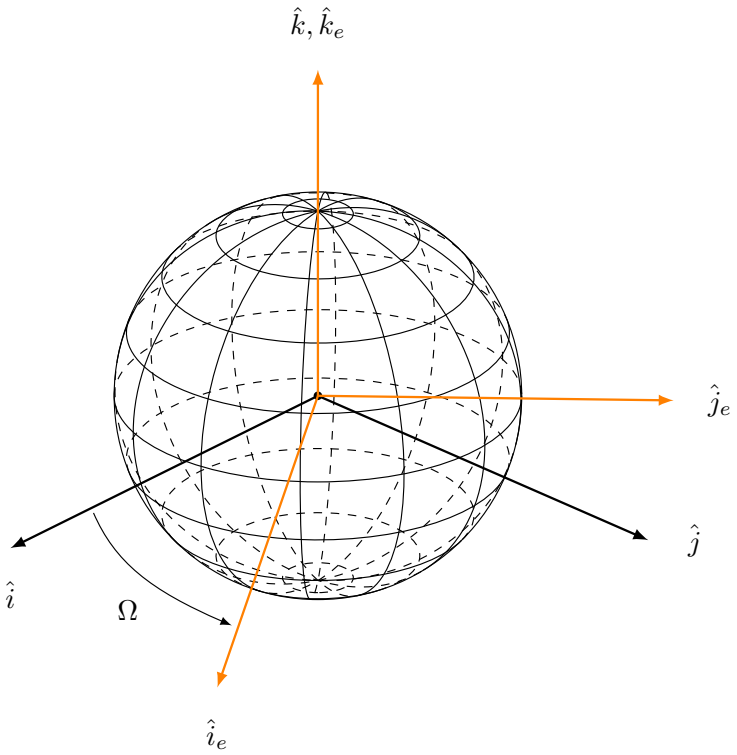

Figure 3.1: Earth centered inertial and Earth centered fixed reference frames

The relation between ECF and ECI visible in figure 3.1 is determined by the Earth's rotation about the $\hat{k}$ vector for the angle between vernal equinox in J2000 and Greenwich meridian (i.e. from $\hat{i}$ to $\hat{i}_e$). The size of the angle can be expressed as $\Omega = \omega_E(t - t_{J2000})$, where $\omega_E = 7.2921 \times 10^{-5}$ rad/s is the angular velocity of the Earth [2], t indicates the current time and t_{J2000} stands for the J2000 epoch. One complete Earth's rotation with respect to the stars takes approximately 23h 56min, a period of time also called one *sidereal day*. The transformation matrix from ECI to ECF frame can be expressed as

$$T_{ECI}^{ECF} = \begin{bmatrix} \cos(\Omega) & \sin(\Omega) & 0 \\ -\sin(\Omega) & \cos(\Omega) & 0 \\ 0 & 0 & 1 \end{bmatrix} \tag{3.1}$$

3.1.3 Earth Geographic Reference Frame

This is the frame in which any position on the Earth's surface can be described. *Longitude* is understood to be positive from the Greenwich meridian to the east, while *latitude* from the equator to the north.

The frame's origin lies at the point of interest on the Earth's surface and orientation is described by a set of basis vectors $\hat{i}_g, \hat{j}_g$ and $\hat{k}_g$. In order to simplify the model, axes of geographic coordinate system are aligned with body frame axes (see 3.1.4) at the launch pad before takeoff. The system's origin thus lies at the launch pad longitude and latitude coordinates. The vector $\hat{i}_g$ is normal to the Earth's surface pointing upward, vector $\hat{k}_g$ points towards the north and $\hat{j}_g$ to the east completing the triad. The frame may be referred to as a *geographic* or *EG* one.

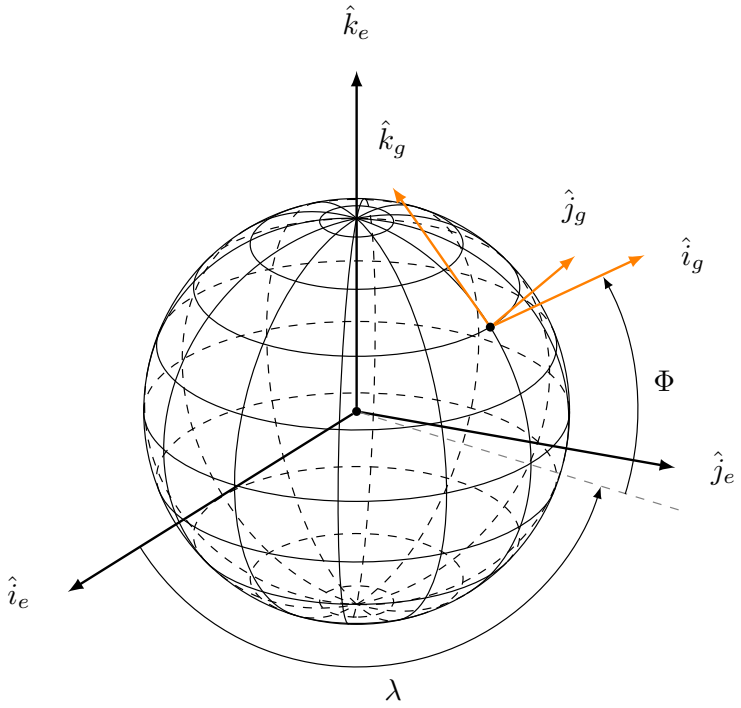

Figure 3.2: Earth centered fixed and Earth geographical reference frames

Transformation from ECF to EG frame consists of two parts and can be further examined in figure 3.2 above. Firstly a rotation about $\hat{k}_e$ (z-axis) for longitude angle λ and secondly rotation about new y-axis for negative latitude angle Φ. The latitude angle is negative in order to achieve the desired orientation of the geographic frame as described above. The total transformation matrix from ECF to EG is formulated as

$$T_{ECF}^{EG} = R(y, -\Phi)R(z, \lambda) \tag{3.2}$$

$$T_{ECF}^{EG} = \begin{bmatrix} \cos(\lambda)\cos(\Phi) & \cos(\Phi)\sin(\lambda) & \sin(\Phi) \\ -\sin(\lambda) & \cos(\lambda) & 0 \\ -\cos(\lambda)\sin(\Phi) & -\sin(\lambda)\sin(\Phi) & \cos(\Phi) \end{bmatrix} \tag{3.3}$$

3.1.4 Body Reference Frame

The last of the four frames is used to describe relative attitude of the launch vehicle with respect to its initial position at the launch pad and serves as a basis for reference points inside the vehicle.

Traditionally in space industry, the body frame is defined by basis vectors $\hat{i}_b, \hat{j}_b$ and $\hat{k}_b$ set as follows. The frame's origin is merged with the spacecraft's center of gravity (*c.g.*), otherwise called the center of mass. Vector $\hat{i}_b$ is aligned with the body main symmetry axis pointing towards the rocket's nose. Coordinate system is further fixed by vector $\hat{j}_b$ aligned with right fin of the rocket and vector $\hat{k}_b$ completes the right-handed triad pointing downwards from the rocket's belly. The body reference frame may be simply called as the *body* one or by abbreviation B.

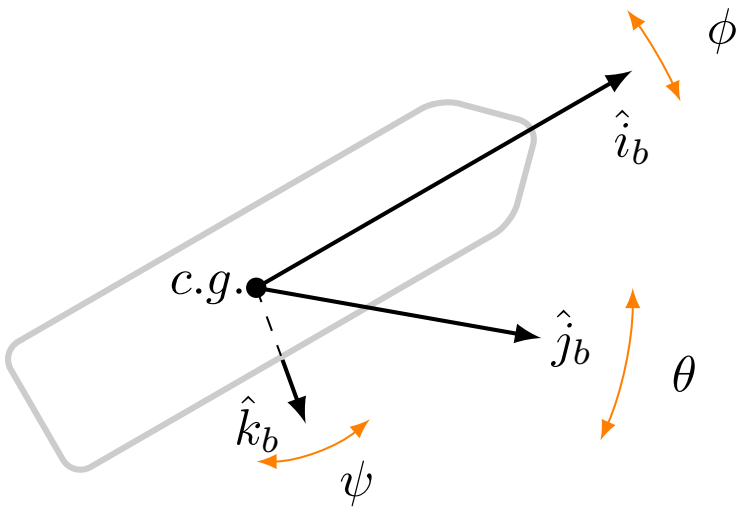

Figure 3.3: Body reference frame with yaw, pitch and roll angles of rotation

Any relative attitude of a body in space can be described using three consecutive rotations about its three main body axis, in our case $\hat{i}_b, \hat{j}_b$ and $\hat{k}_b$. In aerospace industry these axis and angles ψ, θ, ϕ are typically referred to as yaw, pitch and roll successively. Overall orientation of the body frame can be examined in figure 3.3. The total rotation from geographical to body frame can be expressed by transformation matrix

$$T_{EG}^{B} = R(x,\phi)R(y,\theta)R(z,\psi) \tag{3.4}$$

$$T_{EG}^{B} = \begin{bmatrix} \cos(\theta)\cos(\psi) & \cos(\theta)\sin(\psi) & -\sin(\theta) \\ \cos(\psi)\sin(\theta)\sin(\phi) - \cos(\phi)\sin(\psi) & \cos(\phi)\cos(\psi) + \sin(\theta)\sin(\phi)\sin(\psi) & \cos(\theta)\sin(\phi) \\ \sin(\phi)\sin(\psi) + \cos(\phi)\cos(\psi)\sin(\theta) & \cos(\phi)\sin(\theta)\sin(\psi) - \cos(\psi)\sin(\phi) & \cos(\theta)\cos(\phi)] \end{bmatrix} \tag{3.5}$$

Although the inertial frame used throughout this work is the ECI one, there seems to be no point in determining the absolute launch vehicle's attitude with respect to it. Instead, the

yaw, pitch and roll angles (YPR) will describe rocket's attitude with respect to the initial position at the launch pad, to the EG frame.

3.2 Rotational Kinematics

In the previous chapter various reference frames and transformation relations in between them have been discussed. The yaw, pitch and roll angles hold great significance for describing spacecraft attitude and behavior. In order to obtain their values throughout the flight, differential equations are necessary. An angular velocity is introduced as a derivative of the YPR angles. The total angular velocity of launch vehicle's body frame with respect to the geographic reference frame is expressed in body frame coordinates and can be decomposed into three axes components

$$\vec{\omega} = p\hat{i}_b + q\hat{j}_b + r\hat{k}_b \tag{3.6}$$

As we are dealing with rotational angles used in reference frames transformation, the angular velocity can also be represented as shown by *Wie* [3].

$$\vec{\omega} = \begin{bmatrix} p \\ q \\ r \end{bmatrix} \tag{3.7}$$

$$= \begin{bmatrix} \dot{\phi} \\ 0 \\ 0 \end{bmatrix} + R(x,\phi) \begin{bmatrix} 0 \\ \dot{\theta} \\ 0 \end{bmatrix} + R(x,\phi)R(y,\theta) \begin{bmatrix} 0 \\ 0 \\ \dot{\psi} \end{bmatrix} \tag{3.8}$$

$$= \begin{bmatrix} \dot{\phi} - \dot{\psi}\sin\theta \\ \dot{\theta}\cos\phi + \dot{\psi}\cos\theta\sin\phi \\ \dot{\psi}\cos\theta\cos\phi - \dot{\theta}\sin\phi \end{bmatrix} \tag{3.9}$$

$$= \begin{bmatrix} 1 & 0 & -\sin\theta \\ 0 & \cos\phi & \sin\phi\cos\theta \\ 0 & -\sin\phi & \cos\phi\cos\theta \end{bmatrix} \begin{bmatrix} \dot{\phi} \\ \dot{\theta} \\ \dot{\psi} \end{bmatrix} \tag{3.10}$$

We have expressed angular velocity using derivatives of YPR angles. However, the inverse situation is more common in real life, and thus from equation 3.10 the kinematic differential equation can be obtained.

$$\begin{bmatrix} \dot{\phi} \\ \dot{\theta} \\ \dot{\psi} \end{bmatrix} = \frac{1}{\cos\theta} \begin{bmatrix} \cos\theta & \sin\phi\sin\theta & \cos\phi\sin\theta \\ 0 & \cos\phi\cos\theta & -\sin\phi\cos\theta \\ 0 & \sin\phi & \cos\phi \end{bmatrix} \begin{bmatrix} p \\ q \\ r \end{bmatrix} \tag{3.11}$$

The biggest drawback of using Euler angles is that any rotational sequence has a singularity at some point. In our case we can see the problem right away from the equation 3.11. It does not make any sense for pitch angle $\theta = \frac{\pi}{2} + k\pi$ where $k \in Z$ because of cosine function in denominator of the fraction. Such singularity is often referred to as a *gimbal lock*, term originally describing a mechanical phenomenon when two axes of rotation coincide causing the system to lose one degree of freedom. In other words, it becomes unrecognizable about which axes of the two the system is rotating [4]. One of the possible solutions is to introduce

quaternions, and thus fully avoid the danger of a gimbal lock. The use of quaternions in computer simulation has also a great advantage of reducing the computation time as the number of demanding trigonometric expressions is cut down.

Rotation quaternion for our rotation sequence $3-2-1$ is described by *Diebel* [4] as

$$\vec{q} = \begin{bmatrix} q_0 \\ q_1 \\ q_2 \\ q_3 \end{bmatrix} = \begin{bmatrix} \cos\frac{\phi}{2}\cos\frac{\theta}{2}\cos\frac{\psi}{2} + \sin\frac{\phi}{2}\sin\frac{\theta}{2}\sin\frac{\psi}{2} \\ \sin\frac{\phi}{2}\cos\frac{\theta}{2}\cos\frac{\psi}{2} - \cos\frac{\phi}{2}\sin\frac{\theta}{2}\sin\frac{\psi}{2} \\ \cos\frac{\phi}{2}\sin\frac{\theta}{2}\cos\frac{\psi}{2} + \sin\frac{\phi}{2}\cos\frac{\theta}{2}\sin\frac{\psi}{2} \\ \cos\frac{\phi}{2}\cos\frac{\theta}{2}\sin\frac{\psi}{2} - \sin\frac{\phi}{2}\sin\frac{\theta}{2}\cos\frac{\psi}{2} \end{bmatrix} \tag{3.12}$$

where q_0 is a scalar and q_1, q_2 and q_3 are forming a vector $\hat{q}$. For total angular velocity $\vec{\omega}$ of the body with respect to EG frame, the rotational kinematics equation 3.11 has its equivalent in quaternions [1] given by

$$\begin{bmatrix} \dot{q}_0 \\ \dot{q}_1 \\ \dot{q}_2 \\ \dot{q}_3 \end{bmatrix} = \frac{1}{2} \begin{bmatrix} 0 & -p & -q & -r \\ p & 0 & r & -q \\ q & -r & 0 & p \\ r & q & -p & 0 \end{bmatrix} \begin{bmatrix} q_0 \\ q_1 \\ q_2 \\ q_3 \end{bmatrix} \tag{3.13}$$

Moreover, any rotational matrix can be built from quaternions with the help of equation

$$R = (q_0^2 - \hat{q}^T\hat{q})I_3 + 2\hat{q}\hat{q}^T + 2q_0[\hat{q}_x] \tag{3.14}$$

where $[\hat{q}_x]$ is the so-called skew-symmetric matrix expressing the cross product operation. If we apply this equation to the transformation from geographical to body frame, the result is an equivalent transformation matrix to the equation 3.5.

$$T_{EG}^{B} = \begin{bmatrix} q_0^2 + q_1^2 - q_2^2 - q_3^2 & 2q_1q_2 - 2q_0q_3 & 2q_0q_2 + 2q_1q_3 \\ 2q_0q_3 + 2q_1q_2 & q_0^2 - q_1^2 + q_2^2 - q_3^2 & 2q_2q_3 - 2q_0q_1 \\ 2q_1q_3 - 2q_0q_2 & 2q_0q_1 + 2q_2q_3 & q_0^2 - q_1^2 - q_2^2 + q_3^2 \end{bmatrix} \tag{3.15}$$

The Euler angles representing yaw, pitch and roll rotations can be obtained back from quaternion notation by three equations

$$\psi = \arctan\left(\frac{2q_1q_2 + 2q_0q_3}{q_0^2 + q_1^2 - q_2^2 - q_3^2}\right) \tag{3.16}$$

$$\theta = \arcsin(-2q_0q_2 + 2q_1q_3) \tag{3.17}$$

$$\phi = \arctan\left(\frac{2q_2q_3 + 2q_0q_1}{q_0^2 - q_1^2 - q_2^2 + q_3^2}\right) \tag{3.18}$$

3.3 Equations of Motion

In this section, the dynamics of the launch vehicle is described accommodating six degrees of freedom, in accordance with *Wu* [5]. Two parts are treated separately, the translational and rotational movement. General equations are set up with respect to various reference frames. Individual parts of the equations will be described in the following sections.

3.3.1 Translational Dynamics

The first three degrees of freedom belong to translational movement. We draw on Newton's second law in the form of

$$\vec{a} = \frac{1}{m}\vec{F} \tag{3.19}$$

As has already been stated in section 3.1, the total position of the launch vehicle is given with respect to the inertial frame and can be described by vector

$$\vec{r} = x\hat{i} + y\hat{j} + z\hat{k} \tag{3.20}$$

The velocity and acceleration in inertial frame are then obtained one by one as

$$\vec{v} = \dot{\vec{r}} = \dot{x}\hat{i} + \dot{y}\hat{j} + \dot{z}\hat{k} \tag{3.21}$$

$$\vec{a} = \dot{\vec{v}} = \ddot{x}\hat{i} + \ddot{y}\hat{j} + \ddot{z}\hat{k} \tag{3.22}$$

That is for the left side of the 3.19 equation. For the right side, we need to sum all the external forces acting on the launch vehicle. Several sources are taken into consideration - atmosphere, gravity and propulsion. The atmospheric (or aerodynamic) forces as well as thrust will be most conveniently expressed in body frame. However, the gravity force varies based on the location on the Earth and, as shown below, can be expressed in both geographical and inertial frame. In equation 3.23 the inertial one is chosen. With the appropriate transformations, we can express first three differential equations as

$$\dot{\vec{v}} = \frac{1}{m}\left[T_B^{ECI}\left(\vec{F}_{atm} + \vec{F}_{thr}\right) + \vec{F}_g\right] \tag{3.23}$$

Next three differential equations are provided simply by the equation

$$\dot{\vec{r}} = \vec{v} \tag{3.24}$$

3.3.2 Rotational Dynamics

Although the 3 DOF simulation treating an object as a point mass is sufficient during an initial mission design, more comprehensive approach is assumed in this work. Three more degrees of freedom are introduced in order to describe the launch vehicle's attitude. While its position is calculated with respect to the ECI inertial frame, the attitude for simulation purposes is measured with respect to the initial position of the spacecraft on the launch pad, i.e. the EG reference frame. This way the yaw, pitch and roll angles are clearly defined.

The Euler's second law can be written as

$$\vec{M} = \dot{\vec{L}} \tag{3.25}$$

where $\vec{M}$ is the sum of external moments/torques acting on the body and $\vec{L}$ represents the angular momentum, in the simplest case about the center of gravity of the body. It can be further deduced that

$$\vec{L} = \hat{J} \cdot \vec{\omega} \tag{3.26}$$

where $\vec{\omega}$ represents total angular velocity of the body and $\hat{J}$ is the moment of inertia expressing how much torque has to be exerted on the body to reach a desired angular acceleration. It can be obtained by integrating the second moments of mass of all body points with respect to their distance d from the rotational axis over the whole body mass M.

$$\hat{J} = \int_M d^2 \, dm \tag{3.27}$$

When spread all over three main body axes x, y, z, tensor $\hat{J}$ consists of three moments of inertia for each of the axes [3].

$$\hat{J} = \begin{bmatrix} \hat{i}_b & \hat{j}_b & \hat{k}_b \end{bmatrix} \begin{bmatrix} J_{11} & J_{12} & J_{13} \\ J_{21} & J_{22} & J_{23} \\ J_{31} & J_{32} & J_{33} \end{bmatrix} \begin{bmatrix} \hat{i}_b \\ \hat{j}_b \\ \hat{k}_b \end{bmatrix} \tag{3.28}$$

Finally, the equation of motion for an object treated as a rigid body can be written in the form of

$$\vec{M} = \hat{J} \cdot \dot{\vec{\omega}} + \vec{\omega} \times (\hat{J} \cdot \vec{\omega}) \tag{3.29}$$

Now we will parse the sum of the external moments acting on the launch vehicle. When proceeding from the previous part, three main sources of forces and torques are considered acting on the spacecraft - atmosphere, gravity and propulsion. Only the gravitational force is acting in the center of gravity of the spacecraft, and thus producing no torque. Moments from atmospheric (aerodynamic) and propulsion forces have different reference points. Correct reference frames have to be maintained. With respect to the moment of inertia tensor, the body frame is chosen as the inertial one this time. The equation 3.29 can be rearranged, the total external moment substituted and with combination of equation 3.13 we obtain another set of seven equations of motion

$$\dot{\vec{\omega}} = (\hat{J})^{-1} \left[\vec{M}_{atm} + \vec{M}_{thr} - \vec{\omega} \times (\hat{J} \cdot \vec{\omega}) \right] \tag{3.30}$$

$$\begin{bmatrix} \dot{q}_0 \\ \dot{q}_1 \\ \dot{q}_2 \\ \dot{q}_3 \end{bmatrix} = \frac{1}{2} \begin{bmatrix} 0 & -p & -q & -r \\ p & 0 & r & -q \\ q & -r & 0 & p \\ r & q & -p & 0 \end{bmatrix} \begin{bmatrix} q_0 \\ q_1 \\ q_2 \\ q_3 \end{bmatrix} \tag{3.13 revisited}$$

3.4 Subsystem Models

Two sets of total thirteen equations of motion were developed throughout the previous section. First one deals with forces and launch vehicle's translational movement in space. The second set considers moments exerted by external forces on spacecraft and their impact on attitude dynamics. Each of the force and moment sources is described in this section.

3.4.1 Gravity

Planet Earth is often pictured as an ideal sphere. However, the reality lies far from that. Our planet is flattened on the poles and thus resembles more of an ellipsoid. In fact, the proper term used for the Earth's shape is called *geoid*. One of the latest geometric estimations of the Earth's shape is the *World Geodetic System 1984* model [6], which is in its simplified form used throughout this work. Our motivation is to describe the variations in gravitational acceleration $\vec{g}$ magnitude based on location around the Earth. The WGS84 ellipsoid is defined by several constants summarized in the table 3.1 below.

Quantity	**Symbol**	**Value**
semi-major axis	a	6,378,137.0 m
mean radius	R_m	6,371,008.8 m
flattening	f	1/298.257223563
eccentricity	e	0.08181919084
gravitational constant	μ	3,986,004.418 $m^3 s^{-2}$

Table 3.1: WGS84 model defining constants

The geographic reference frame introduced in section 3.1.3 works with geocentric latitude Φ_c. In order to determine gravitational acceleration, we need to introduce geodetic latitude Φ_g which is the value commonly seen on maps. The geocentric latitude represents the angle between equatorial plane and the position on spherical Earth surface. On the other hand, geodetic latitude is defined as the angle between equatorial plane and plane tangent to the ellipsoid Earth surface. Relation between geocentric and geodetic latitudes can be quite easily figured out.

$$\tan \Phi_g = \frac{\tan \Phi_c}{(1-f)^2} \tag{3.31}$$

The gravitational acceleration depending on geodetic latitude and altitude above the surface can be then expressed in EG by employing *colatitude* angle $\Upsilon = 90 - \Phi_c$ as follows [7].

$$\begin{aligned} g_r = & -\frac{\mu}{r^2}\left[1 - \frac{3}{2}J_2\Big(\frac{R_0}{r}\Big)^2(3\cos^2\Upsilon - 1) - 2J_3\Big(\frac{R_0}{r}\Big)^3\cos\Upsilon(5\cos^2\Upsilon - 3)\right. \\ & \left. - \frac{5}{8}J_4\Big(\frac{R_0}{r}\Big)^4(35\cos^4\Upsilon - 30\cos^2\Upsilon + 3)\right] \end{aligned} \tag{3.32}$$

$$\begin{aligned} g_\Upsilon = & -3\frac{\mu}{r^2}\Big(\frac{R_0}{r}\Big)^2\sin\Upsilon\cos\Upsilon\left[J_2 + \frac{1}{2}J_3\Big(\frac{R_0}{r}\Big)\sec\Upsilon(5\cos^2\Upsilon - 3)\right] \\ & + \frac{5}{6}J_4\left[\Big(\frac{R_0}{r}\Big)^2(7\cos^2\Upsilon - 3)\right] \end{aligned} \tag{3.33}$$

where J_i are so called oblateness terms estimating the geoid shape: $J_2 = 1.0826 \times 10^{-3}$, $J_3 = -2.54 \times 10^{-6}$ and $J_4 = -1.61 \times 10^{-6}$ and reference ellipsoid radius is approximated by equation

$$R_0 = a\left[1 - \frac{e}{2}(1 - \cos 2\Phi_g) + \frac{5}{16}e^2(1 - \cos 4\Phi_g)\right] \tag{3.34}$$

Moreover, gravitational acceleration can be also expressed in ECI inertial frame using Cartesian coordinates, which may be useful during latter simulation. Terms higher than J_2 are neglected here [7]. If the total gravitational acceleration is represented by vector

$$\vec{g} = g_x\hat{i} + g_y\hat{j} + g_z\hat{k} \tag{3.35}$$

then its individual components can be calculated as

$$g_x = -\frac{\mu}{r^2}\left[1 + \frac{3}{2}J_2\Big(\frac{R_0}{r}\Big)^2\left[1 - 5\Big(\frac{z}{r}\Big)^2\right]\right]\frac{x}{r} \tag{3.36}$$

$$g_y = -\frac{\mu}{r^2}\left[1 + \frac{3}{2}J_2\Big(\frac{R_0}{r}\Big)^2\left[1 - 5\Big(\frac{z}{r}\Big)^2\right]\right]\frac{y}{r} \tag{3.37}$$

$$g_z = -\frac{\mu}{r^2}\left[1 + \frac{3}{2}J_2\Big(\frac{R_0}{r}\Big)^2\left[3 - 5\Big(\frac{z}{r}\Big)^2\right]\right]\frac{z}{r} \tag{3.38}$$

The total gravitational acceleration is for lower altitudes almost directly proportional to the altitude.

Finally, gravitational force affecting the spacecraft of total mass m is established.

$$\vec{F}_g = \begin{bmatrix} F_{g_x} \\ F_{g_y} \\ F_{g_z} \end{bmatrix} = m \begin{bmatrix} g_x \\ g_y \\ g_z \end{bmatrix} \tag{3.39}$$

Gravitational force has its point of application in the center of gravity of the launch vehicle. Thus, it produces no torque on the launch vehicle about the c.g. which is the origin of our body frame.

3.4.2 Atmosphere

This work is focused on a lift-off phase of flight in the Earth's atmosphere which cannot be compared to a free space flight. Atmosphere plays a significant role in the real flight and thus must be taken into consideration in the mathematical model.

As the launch vehicle ascends upward, it flies through several distinct layers of atmosphere. Each of them has unique properties and the rate of change in pressure, temperature or air density varies with altitude. Primarily, air density characteristics is crucial for describing forces acting on the spacecraft, as we will see later. Simplified calculations based on the *U.S. Standard Atmosphere 1976* model [8] are introduced here. The model itself uses a very broad set of equations and tables to precisely describe atmospheric variations over an altitude and its implementation is beyond our topic. Therefore, some simplifications have been made. However, the work can always be built on and expanded with more precise models.

The air pressure is approximated by equation

$$p = p_0 \left(1 - \frac{Lh}{T_0}\right)^{\frac{gM}{RL}} \tag{3.40}$$

where $p_0 = 101325\ Pa$ is the sea level pressure, $L = 0.0065\ Km^{-1}$ is the molecular scale temperature gradient, $h\ [m]$ is the the altitude above ground, $T_0 = 288.15\ K$ is the sea level temperature, $g\ [ms^{-2}]$ is the gravitational acceleration magnitude at current position obtained from gravity model, $M = 0.028964\ kgmol^{-1}$ is the molar mass of air and $R = 8.31447\ JK^{-1}mol^{-1}$ is the universal ideal gas constant. Note that these variables are not constant in real life and vary slightly with altitude. Nevertheless, for the purpose of our air pressure model, they are considered to be constant.

The dependence of the air pressure on altitude above the Earth's surface with general $g = 9.80665\ ms^{-2}$ is plotted in figures 3.4 and 3.5 on the next page.

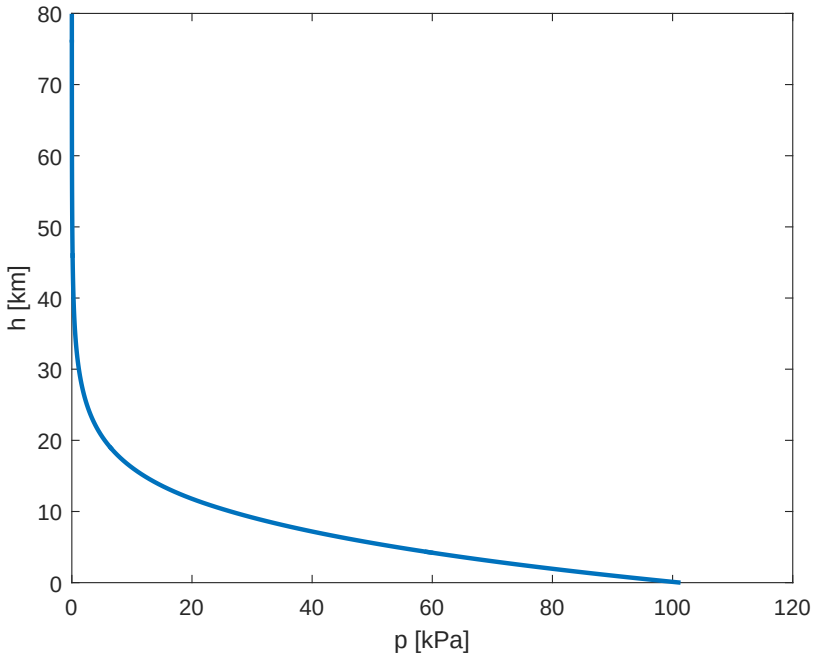

Figure 3.4: Air pressure as a function of altitude up to 80 km

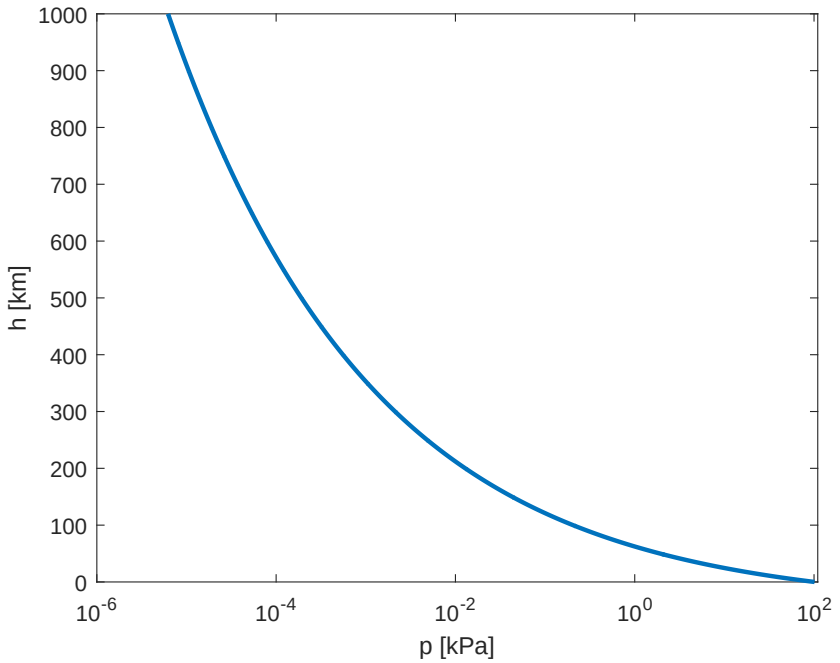

Figure 3.5: Air pressure as a function of altitude up to 1000 km

The temperature varies abruptly over several distinct atmospheric layers up to the altitude of 120 km and then follows exponential curve. The equations for each of the layers are fully described below [8].

- For altitude from sea level up to $h = 86\ km$, the temperature can be approximated by the equation
$$T = T_{0_b} - L_b(h - h_b) \tag{3.41}$$
where L is picked from the table 3.2 below based on the current altitude for each of the atmospheric layers and T_0 is simply the temperature at the borders between obtained from previous calculations; for $b = 0$ is $T_0 = 288.15\ K$.

b	$h_b\ [km]$	$L\ [K]$
0	0	-6.5
1	11	0.0
2	20	$+1.0$
3	32	$+2.8$
4	47	0.0
5	51	-2.8
6	71	-2.0
7	86	$-$

Table 3.2: Constants defining atmospheric layers

- For altitude from 86 km to 91 km, the temperature remains constant at value
$$T = 186.8673\,K \tag{3.42}$$
- For altitude from 91 km up to 110 km, the temperature is approximated as an elliptic curve expressed by
$$T = 263.1905 - 76.3232\left[1 - \left(\frac{h - 91}{-19.9429}\right)^2\right]^{1/2} \tag{3.43}$$
where all the values used are defined constants.
- For altitude from 110 km to 120 km the temperature is governed by the equation
$$T = 240 + 12(h - 110) \tag{3.44}$$
- Finally, for altitude from 120 km up to 1000 km which is more than sufficient for our purposes, the temperature has an exponential form of
$$T = T_{\text{inf}} - (T_{\text{inf}} - 360)\exp(-0.01875\zeta) \tag{3.45}$$

where $T_{\text{inf}} = 1000\ K$ and ζ is defined with the help of $r_0 = 6.356766 \times 10^6\ km$ as

$$\zeta = (h - 120)\Big(\frac{r_0 + 120}{r_0 + h}\Big) \tag{3.46}$$

We have fully described the temperature model as stated in U.S. Standard Atmosphere 1976 model [8]. The dependence of temperature on altitude above the Earth's surface with general $g = 9.80665\ m/s^2$ is plotted in figures 3.6 and 3.7 below.

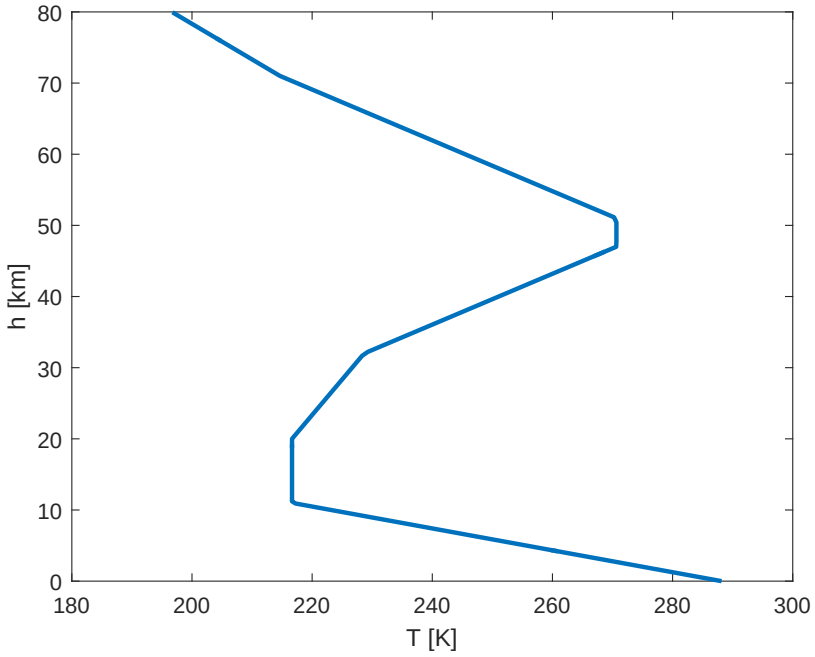

Figure 3.6: Air temperature as a function of altitude up to 80 km

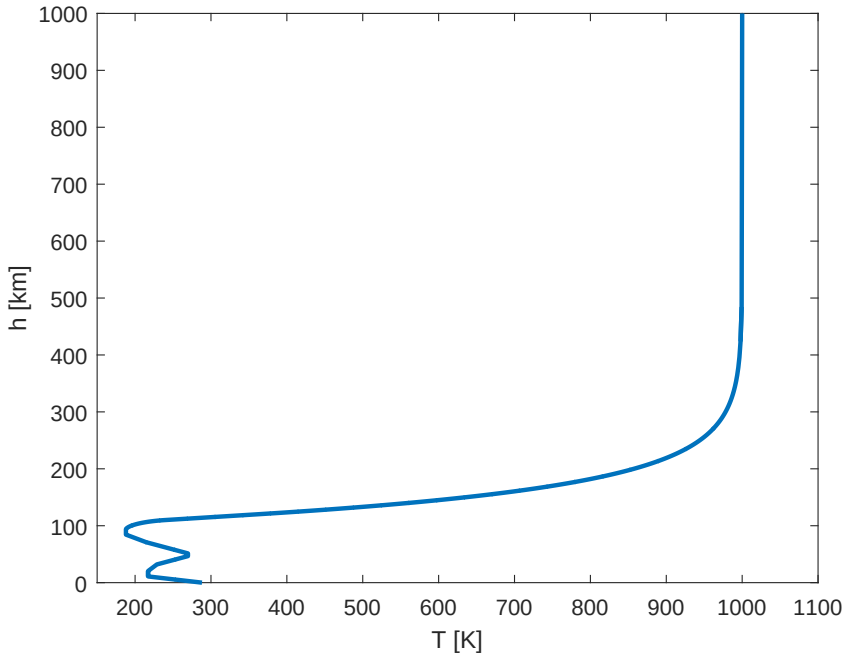

Figure 3.7: Air temperature as a function of altitude up to 1000 km

The air mass density can now be calculated using pressure and temperature values at certain altitude as

$$\rho = \frac{pM}{RT} \tag{3.47}$$

The dependence of air mass density on altitude above the Earth's surface with general $g = 9.80665\ m/s^2$ is plotted in figures 3.8 and 3.9 on the next page.

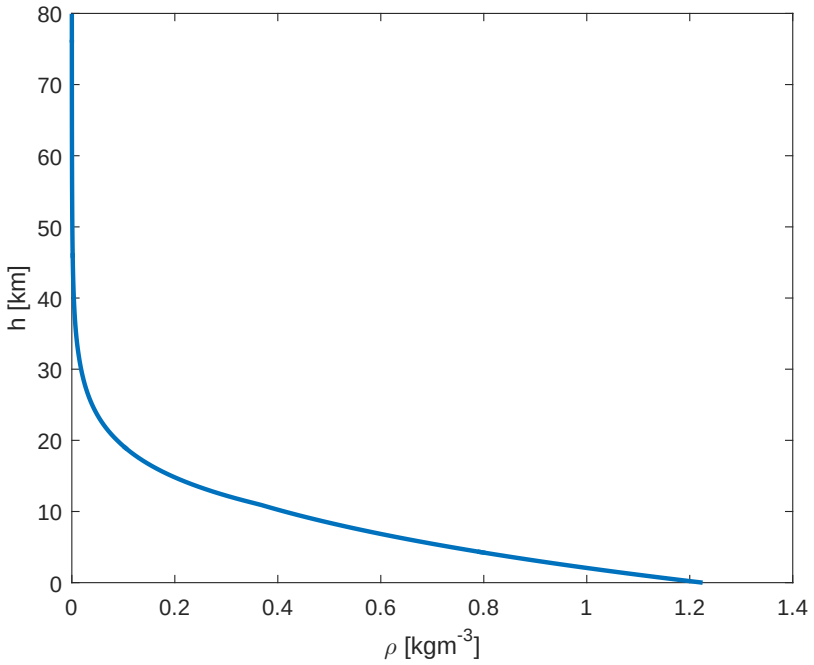

Figure 3.8: Air mass density as a function of altitude up to 80 km

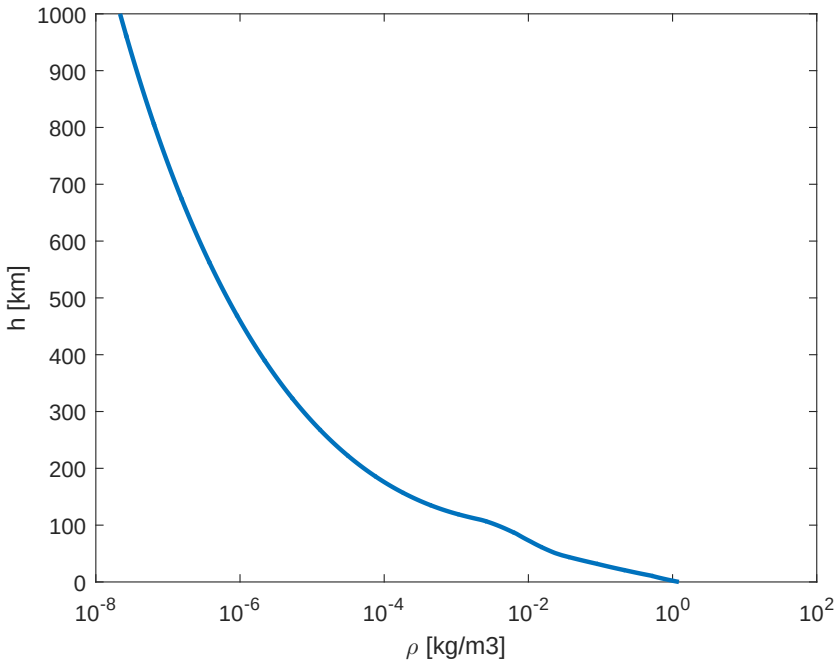

Figure 3.9: Air mass density as a function of altitude up to 1000 km

With air density determined at any altitude, the forces acting on a spacecraft in the atmosphere can be presented. When we speak about aerodynamic forces, we usually mean *lift* and *drag*. Lift L is a force acting upward, normal to the direction of flight. Drag D is pointing backward, in opposite to the velocity. However, when dealing with bodies symmetrical along the main axis of rotation such as rockets or missiles, different set of forces may be easier to employ. Those forces are called *normal* and *axial* and they are defined in the body frame, which brings us some benefits. The normal force N is acting upward, normal to the $\hat{i}_b$ body axis. Axial force A is pointing backward, along the main body axis $\hat{i}_b$. A third force perpendicular to both of the previous forces is called *side* force S and remains unchanged.

Relation between the two sets of forces is guided by an *angle of attack* α, the angle between the relative air mass velocity and the main body axis $\hat{i}_b$, as can be seen in figure 3.10 below. The second angle determining the spacecraft's orientation towards the air mass velocity is *side slip angle* β. The angle of attack is defined as

$$\alpha = \tan^{-1}\left(\frac{v_{air_z}}{v_{air_x}}\right) \tag{3.48}$$

and the side slip angle as

$$\beta = \tan^{-1}\left(\frac{v_{air_y}}{v_{air_x}}\right) \tag{3.49}$$

Assuming that the air mass surrounding the vehicle is still in relation to the ground and any disturbances such as wind are neglected, the relative velocity is equal to the vehicle's velocity

$$\vec{v}_{air} = \vec{v} \tag{3.50}$$

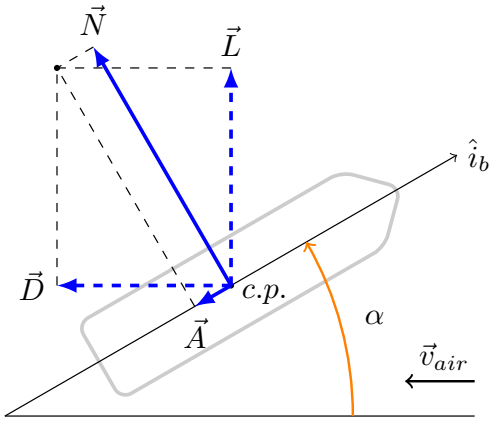

Figure 3.10: Relation between lift & drag and normal & axial forces acting on a body

We can transform from the pair of drag and lift to normal and axial forces using the equations

$$N = L\cos(\alpha) + D\sin(\alpha) \tag{3.51}$$

$$A = -L\sin(\alpha) + D\cos(\alpha) \tag{3.52}$$

and vice versa

$$L = N\cos(\alpha) - A\sin(\alpha) \tag{3.53}$$
$$D = N\sin(\alpha) + A\cos(\alpha) \tag{3.54}$$

Aerodynamic forces act on the spacecraft at its center of pressure (*c.p.*) and can be all expressed in a similar form as

$$A = C_A \frac{1}{2}\rho S v_{air}^2 \tag{3.55}$$
$$S = C_S \frac{1}{2}\rho S v_{air}^2 \tag{3.56}$$
$$N = C_N \frac{1}{2}\rho S v_{air}^2 \tag{3.57}$$

where C_N is the normal coefficient, C_A is the axial coefficient and C_S is the side coefficient, ρ $[kgm^{-3}]$ is the air mass pressure at current altitude, S $[m^2]$ is the reference area and $\vec{v}_{air}$ $[ms^{-1}]$ is the velocity of the spacecraft relative to the surrounding air mass.

The aerodynamic coefficients are in reality not constant as we assume them to be. Their dependency on Mach number, angle of attack and side slip angle needs to be determined experimentally or by using complex Computational Fluid Dynamics simulations. For our purposes, we can define them as

$$C_A = C_{A_0} + \alpha C_{A_\alpha} + \beta C_{A_\beta} \tag{3.58}$$
$$C_S = C_{S_0} + \beta C_{S_\beta} \tag{3.59}$$
$$C_N = C_{N_0} + \alpha C_{N_\alpha} \tag{3.60}$$

However, constant values C_{S_0} and C_{N_0} are neglected in further work.

All necessary parts were developed and we can now express the atmospheric aerodynamic forces in body coordinates as

$$\vec{F}_{atm} = \begin{bmatrix} F_{atm_x} \\ F_{atm_y} \\ F_{atm_z} \end{bmatrix} = \begin{bmatrix} -A \\ S \\ -N \end{bmatrix} \tag{3.61}$$

In order to define the moments exerted by aerodynamic forces on the launch vehicle, the location of the center of pressure as their point of reference needs to be clarified. The body frame has its origin located at the center of gravity and to maintain rocket stability the center of pressure has to be located behind it - negative x coordinate in the body reference frame. Let's define position of c.p. in the body coordinates as $\vec{r}_{c.p.} = \begin{bmatrix} -x_{c.p.} & 0 & 0 \end{bmatrix}^T$. However, the aerodynamic moments about the c.g. are usually called yaw, pitch and roll moments

$$\vec{M}_{atm} = \begin{bmatrix} M_{atm_x} \\ M_{atm_y} \\ M_{atm_z} \end{bmatrix} = \vec{r}_{c.p.} \times \vec{F}_{atm} = \begin{bmatrix} M_{roll} \\ M_{pitch} \\ M_{yaw} \end{bmatrix} \tag{3.62}$$

and they are expressed in a similar way as aerodynamic forces

$$M_{roll} = C_{Mr}\frac{1}{2}\rho S v_{air}^2 l \tag{3.63}$$

$$M_{pitch} = C_{Mp}\frac{1}{2}\rho S v_{air}^2 l \tag{3.64}$$

$$M_{yaw} = C_{My}\frac{1}{2}\rho S v_{air}^2 l \tag{3.65}$$

where l $[m]$ is the reference body length and the aerodynamic coefficients dependent on the angle of attack, side slip angle and vehicle's angular velocity are described as

$$C_{Mr} = pC_{Mr_p} \tag{3.66}$$

$$C_{Mp} = \alpha C_{Mp_\alpha} + qC_{Mp_q} \tag{3.67}$$

$$C_{My} = \beta C_{My_\beta} + rC_{My_r} \tag{3.68}$$

It has been proven that when the aerodynamic forces are applied at certain location along the body, the magnitudes of aerodynamic moments remain almost constant, independently of the angle of attack. Such position is called the aerodynamic center [9]. The position of c.p. has to be determined experimentally from the relation 3.62.

3.4.3 Fin Control

One of the options how to steer a launch vehicle is implementing a fin control. Fins are used commonly on rockets for stabilization during flight. On our water rocket model described in greater detail in chapter 5, two sets of fins are used. There are four orthogonal fins at the bottom for passive stabilization and four orthogonal controlled fins close to the rocket head for active flight control. The fins arrangement can be explored on the following sketch.

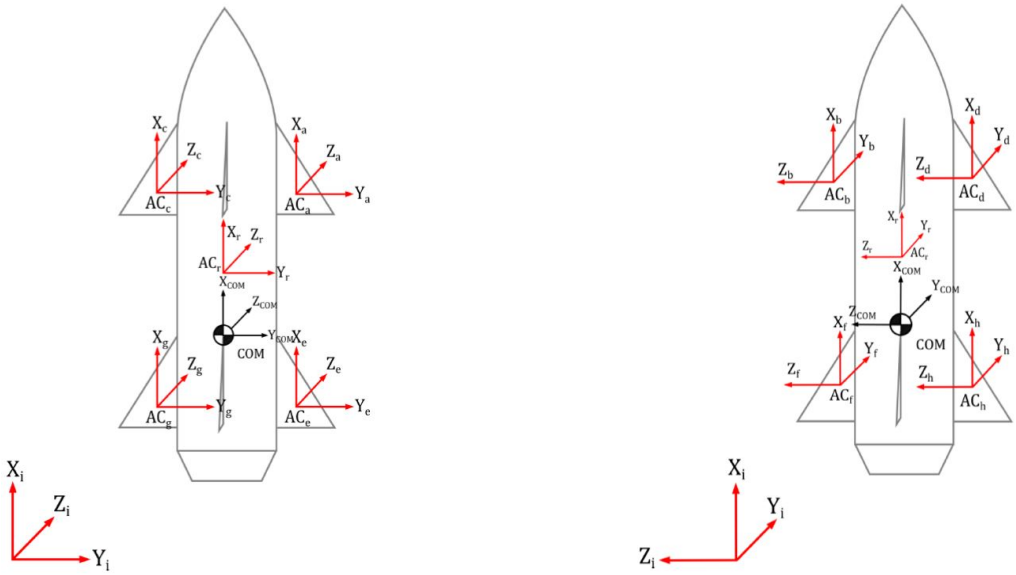

Figure 3.11: Water rocket model fins arrangement [10]

Position of all four steerable fins A, B, C and D is defined by vectors from rocket's c.g. to the geometric center of each fin $\vec{r}_{fin_A}$, $\vec{r}_{fin_B}$, $\vec{r}_{fin_C}$ and $\vec{r}_{fin_D}$. The aerodynamic forces acting on fins are similar to the three dimensional forces acting on the whole spacecraft. However, due to the fins arrangement around the body, one of the three forces can be neglected while one fin is always hidden behind the launch vehicle's body. Thus, for each fin we obtain a pair of forces - axial and side or axial and normal. Specifically, for fins A and C we take into consideration axial and normal forces and for fins B and D axial and side ones.

Although the fins' aerodynamic forces depend on the air velocity and pressure which varies with altitude, the quantities are assumed to be constant for simulation purposes. The forces vary only with the fin turn angle. Apart from that, the equations are equivalent to those developed above, see equation 3.61.

3.4.4 Thrust

Enough of forces hindering our launch vehicle! What drives it up to the sky is propulsion. There are plenty of propulsion types used in aerospace industry but so far only the rocket engines has been suitable for big launch vehicles due to their high thrust level. Simply said, they work by expanding high pressurized gas through a converging-diverging nozzle and thus accelerating propellant to hypersonic velocities [11].

The thrust of such rocket motor is basically given by the equation

$$T = \dot{m}V_e + (p_e - p_a)A_e \tag{3.69}$$

where T $[N]$ is the thrust force, $\dot{m}$ $[kgs^{-1}]$ is the propellant mass flow rate, V_e $[ms^{-1}]$ is the exhaust velocity at nozzle exit, p_e $[Pa]$ is the exhaust pressure at nozzle exit, p_a $[Pa]$ is the ambient pressure equal to zero in vacuum and A_e $[m^2]$ the nozzle exit area which is usually fixed.

Thrust is by no way constant as it depends on ambient pressure which varies with altitude. The higher the rocket flies, the higher thrust we get with some limitations. In order to compare power of different rocket engines, equivalent exhaust velocity is introduced

$$V_{eq} = \frac{T}{\dot{m}} \tag{3.70}$$

as well as specific impulse describing the rate of thrust which is gained from an engine for unit propellant mass flow rate in sea level gravity g_0. Specific impulse is the primary measurement of rocket performance and can always be found in the engine's specifications.

$$I_{sp} = \frac{T}{\dot{m}g_0} = \frac{V_{eq}}{g_0} \tag{3.71}$$

The thrust vectoring is considered the main control mechanism in our model. Engine nozzle is attached to gimbals which can be turned around slightly in all directions, steering the rocket. Two independent angles are responsible for the nozzle attitude - δ_ψ represents rotation of nozzle about yaw axis $\hat{k}_b$ and δ_θ represents rotation of nozzle about pitch axis $\hat{j}_b$ in body coordinates as seen in figure 3.12. Thus only pitch and yaw angles can be controlled by thrust vectoring.

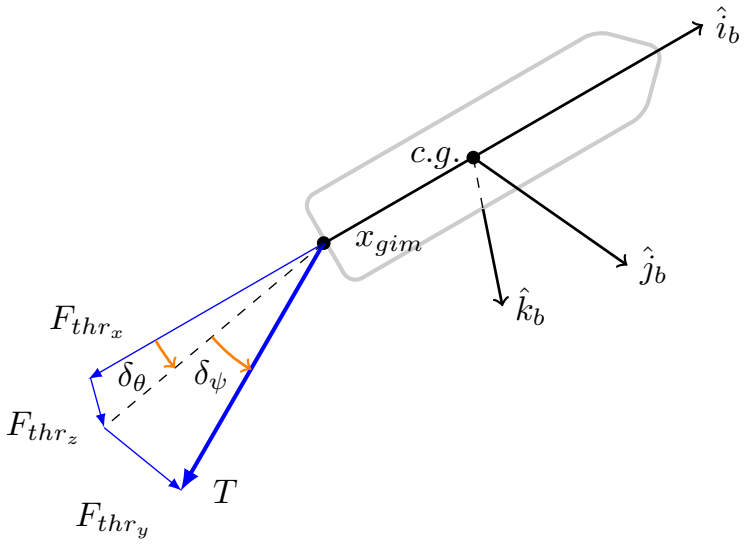

Figure 3.12: Thrust vectoring schema with yaw and pitch control angles

$$\vec{F}_{thr} = \begin{bmatrix} F_{thr_x} \\ F_{thr_y} \\ F_{thr_z} \end{bmatrix} = \begin{bmatrix} T\cos\delta_\psi\cos\delta_\theta \\ T\sin\delta_\psi \\ T\sin\delta_\theta \end{bmatrix} \tag{3.72}$$

Thrust force has its point of action placed where the gimbaled nozzle is connected to the launch vehicle. Such location can be expressed in the body reference frame by vector $\vec{r}_{gim} = \begin{bmatrix} -x_{gim} & 0 & 0 \end{bmatrix}^T$. Total moment exerted on the spacecraft by thrust force is zero when no thrust vectoring is in action. In other cases the moment is non-zero.

$$\vec{M}_{thr} = \begin{bmatrix} M_{thr_x} \\ M_{thr_y} \\ M_{thr_z} \end{bmatrix} = \vec{r}_{gim} \times \vec{F}_{thr} \tag{3.73}$$

Chapter 4

Simulation

Based on the four differential equations fully describing both translational and rotational movement of the launch vehicle a computer based simulation model can be developed. The powerful MATLAB has been employed with combination of Simulink graphical modeling environment. The main nonlinear equations 3.23, 3.24 and 3.30, 3.13 are repeated here for reference.

$$\dot{\vec{v}} = \frac{1}{m}\left[T_B^{ECI}\left(\vec{F}_{atm} + \vec{F}_{thr}\right) + \vec{F}_g\right] \qquad \text{(3.23 revisited)}$$

$$\dot{\vec{r}} = \vec{v} \qquad \text{(3.24 revisited)}$$

$$\dot{\vec{\omega}} = (\hat{J})^{-1}\left[\vec{M}_{atm} + \vec{M}_{thr} - \vec{\omega} \times \hat{J} \cdot \vec{\omega}\right] \qquad \text{(3.30 revisited)}$$

$$\begin{bmatrix} \dot{q}_0 \\ \dot{q}_1 \\ \dot{q}_2 \\ \dot{q}_3 \end{bmatrix} = \frac{1}{2} \begin{bmatrix} 0 & -p & -q & -r \\ p & 0 & r & -q \\ q & -r & 0 & p \\ r & q & -p & 0 \end{bmatrix} \begin{bmatrix} q_0 \\ q_1 \\ q_2 \\ q_3 \end{bmatrix} \qquad \text{(3.13 revisited)}$$

4.1 Simulink Model

At first, each of the subsystems has been modeled and, wherever possible, a block from Simulink library has been used for greater precision, mostly from *Aerospace Blockset*. For example, gravitational acceleration is obtained from *Zonal Harmonic Gravity Model* block and atmospheric data from *COESA Atmosphere Model* block (1976 U.S. Standard Atmosphere). Further mathematical relations are then modeled using standard building blocks. The launch vehicle's flight complex Simulink model is closely interconnected making any debugging quite tricky. A couple of screen shots of various parts of the whole design are presented below in figures 4.1 and 4.2.

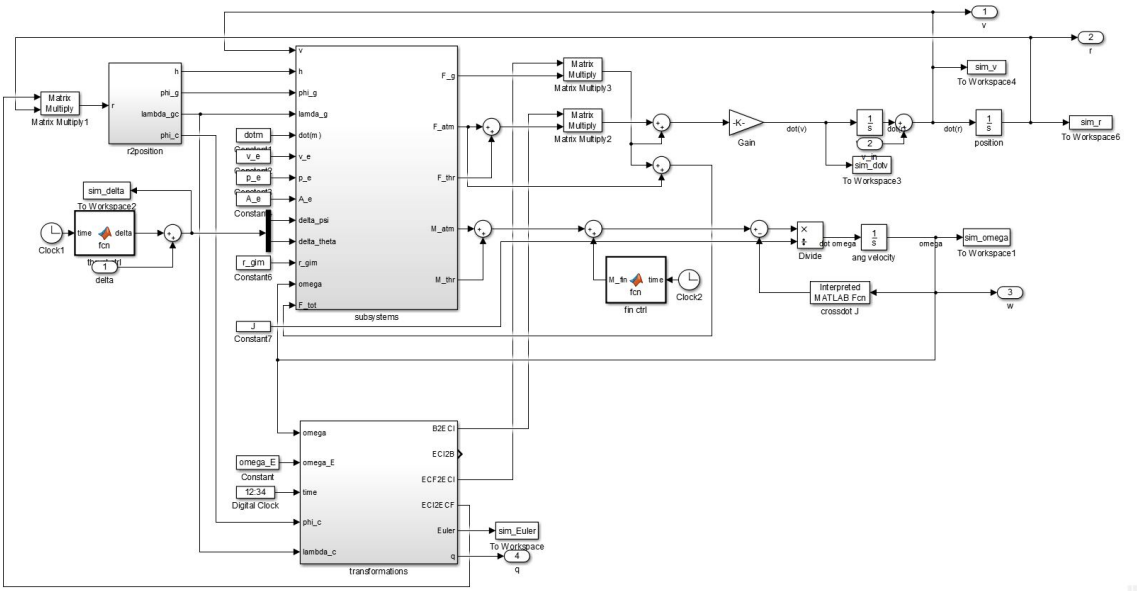

Figure 4.1: Simulink model - main scheme

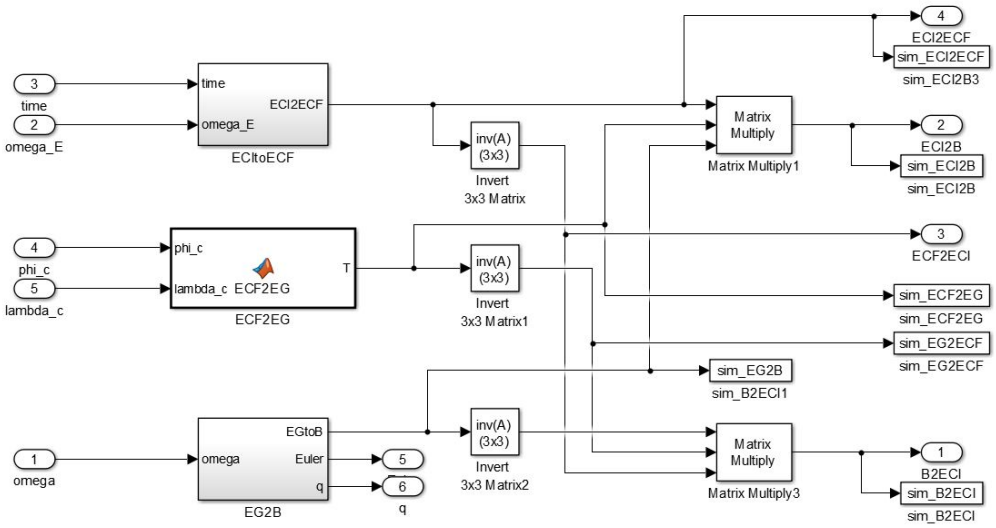

Figure 4.2: Simulink model - transformations

The Simulink model has been designed with the thought of possible future extensions, and thus should be transparent and easily editable. Setting of thrust vectoring and fins control commands has to be done in the Simulink model itself (function blocks `thrust ... ctrl` and `fins ctrl`). The simulation run time is set to 200 s by default, while the engines burn time t_{burn} is 162 s. However, there is no problem of adjusting the simulation run time.

4.2 Input Data

Building a numerical model entails the need for real data. A launch vehicle's flight cannot be simulated without knowing for example the body mass. In order to ensure some level of model's reliability, wide research has been conducted resulting in a partial set of numerical values summarized in the table 4.1 bellow. Most of the data has been taken from the revolutionary Falcon 9 FT launch vehicle of the SpaceX private company. However, some values are simply not available to public, and thus had to be estimated. Those are signed with $\sim$. Real world values are mostly taken from [12], [13] and estimations are based on data obtained from [14].

Quantity	**Symbol**	**Value**	$\sim$
LV mass	m	$570,000\ kg$	
LV length	d	$70\ m$	
Position of gimbal	$\vec{r}_{gim}$	$\begin{bmatrix}-21 & 0 & 0\end{bmatrix}^T$	$\sim$
Main moments of inertia	J_{11}, J_{22}, J_{33}	1.4×10^5, 3.2×10^7, 3.2×10^7	$\sim$
Aerodynamic reference area	S	$21\ m^2$	$\sim$
Reference length	l	$3.24\ m$	$\sim$
Axial force coefficient	C_A	0.2	$\sim$
Axial force coefficient for α	C_{A_α}	0.05	$\sim$
Axial force coefficient for β	C_{A_β}	0.05	$\sim$
Side force coefficient	C_S	0	$\sim$
Side force coefficient for β	C_{S_β}	0.9	$\sim$
Normal force coefficient	C_{N_0}	0	$\sim$
Normal force coefficient for α	C_{N_α}	0.9	$\sim$
Roll moment coefficient for p	C_{Mr_p}	0.8	$\sim$
Pitch moment coefficient for α	C_{Mp_α}	0.05	$\sim$
Pitch moment coefficient for q	C_{Mp_q}	0.8	$\sim$
Yaw moment coefficient for β	C_{My_β}	0.05	$\sim$
Yaw moment coefficient for r	C_{My_r}	0.8	$\sim$
Total thrust	T	$9 \times 845000\ N$	
Specific impulse	I_{sp}	$282\ s$	
Burn time	t_{burn}	$162\ s$	
Exit pressure	p_e	$9 \times 10^5\ Pa$	$\sim$
Nozzle exit area	A_e	$0.97\ m^2$	

Table 4.1: Simulation model input data

Unknown values have been estimated to the best of my knowledge and belief with respect to meaningful outcomes of the simulation as a whole. It should be mentioned that the results highly depend on the initial setup of the numerical values, and thus different outcomes may be obtained from different setups. The Simulink model has to be tuned extensively in order to represent the real world.

Several assumptions have been made along the simulation process. Only moments of inertia about the main rotational axes are considered in the Simulink model. The aerodynamic coefficients from the table 4.1 above are considered to be constants optimized for velocities around 600 m/s. The launch vehicle's body is considered to be rigid.

4.3 Outcomes

Apart from exploring the mathematical equations and code files itself, the best way how to get acquainted with the model is to investigate some results. Flight data from the simulation are presented here in the form of 2D and 3D plots. In order to visualize more features of the model, thrust vectoring is utilized.

Most if not all of the quantities from Simulink model are saved to MATALB's workspace for further analysis. The variables are usually named as `sim_(quantity name)`, for example `sim_phi_c`. Each particular case needs to be checked prior to manipulation with the variables.

Our mathematical model encapsulates several accurate sub models, for example the atmospheric model or thrust model, the output of which can be seen in figure 4.3 bellow.

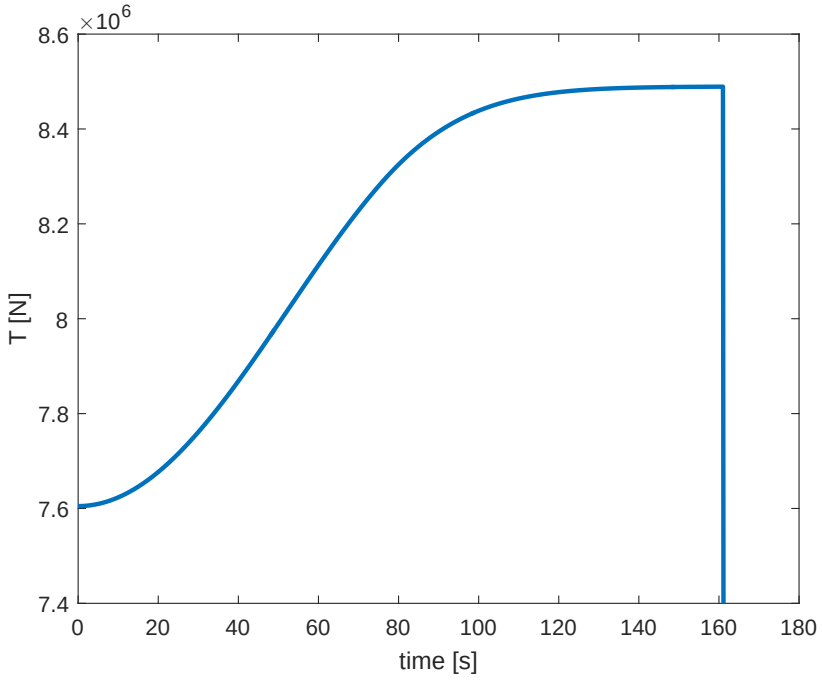

Figure 4.3: Total thrust of all nine rocket engines over time ($t_{burn} = 162\ s$)

However, it was found that the launch vehicle's behavior varies extensively over the whole flight. Due to the changes in air density, rocket's thrust and velocity, the flight cannot be trustworthily simulated with a single set of aerodynamic coefficients that highly influence the

vehicle's dynamics. The coefficients are in reality far from being constants as we perceive them for our purposes. Their values depend heavily on velocity (Mach number). Such complexity is beyond the capabilities of this work. If we perceive aerodynamic coefficients as constants, they are applicable only for some velocities. For simpler simulation cases, the thrust was set equal to dragging forces and velocity is maintained at a constant value. The variations in air density were also neglected. Several significant plots demonstrating the launch vehicle's test flight can be seen in figures 4.4 to 4.7 bellow.

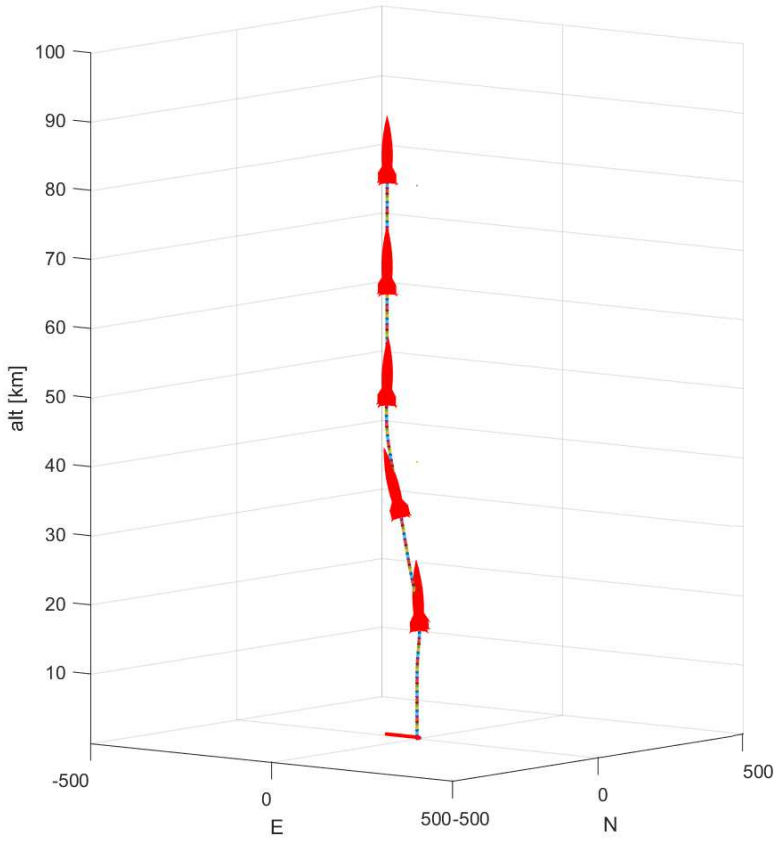

Figure 4.4: Flight trajectory of launch vehicle

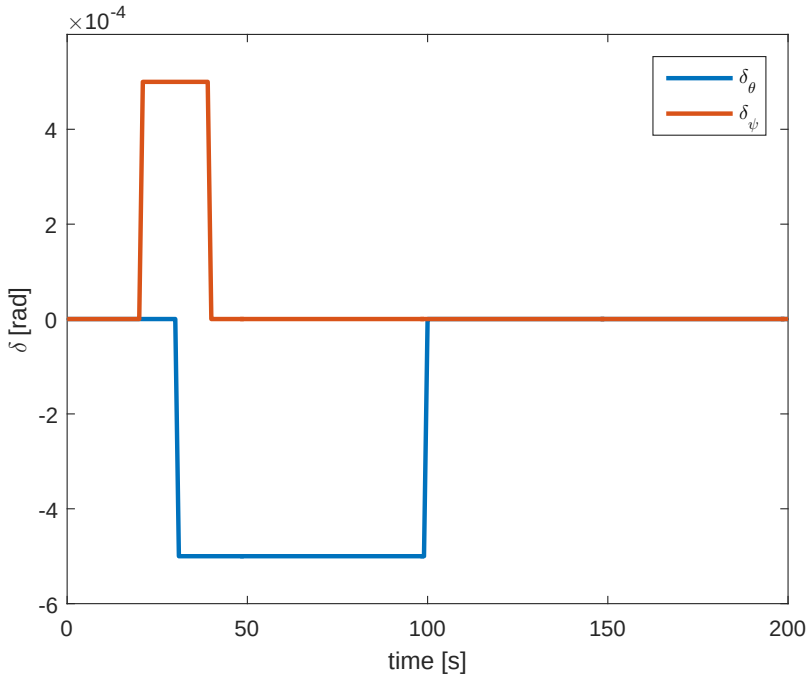

Figure 4.5: Thrust vectoring over time

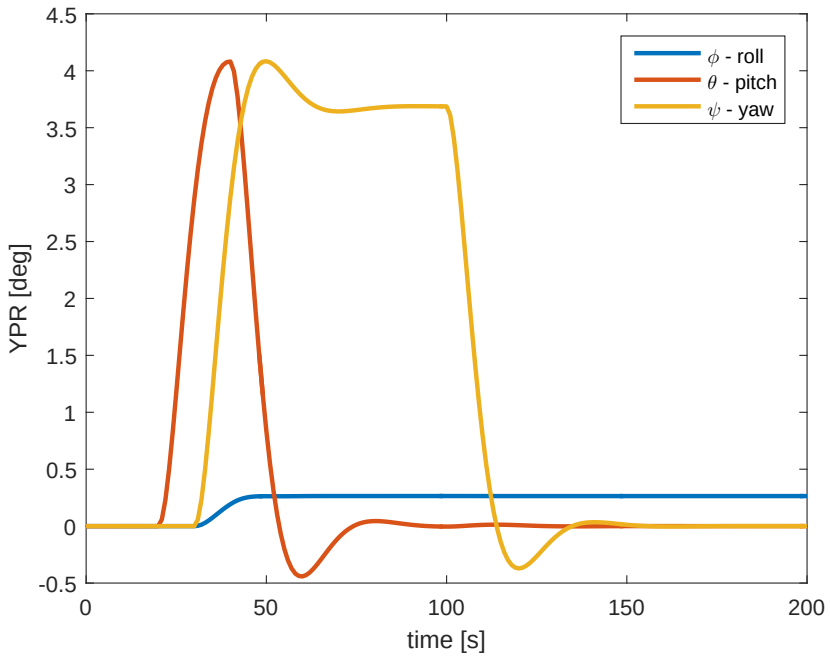

Figure 4.6: Vehicle's Euler angles over time

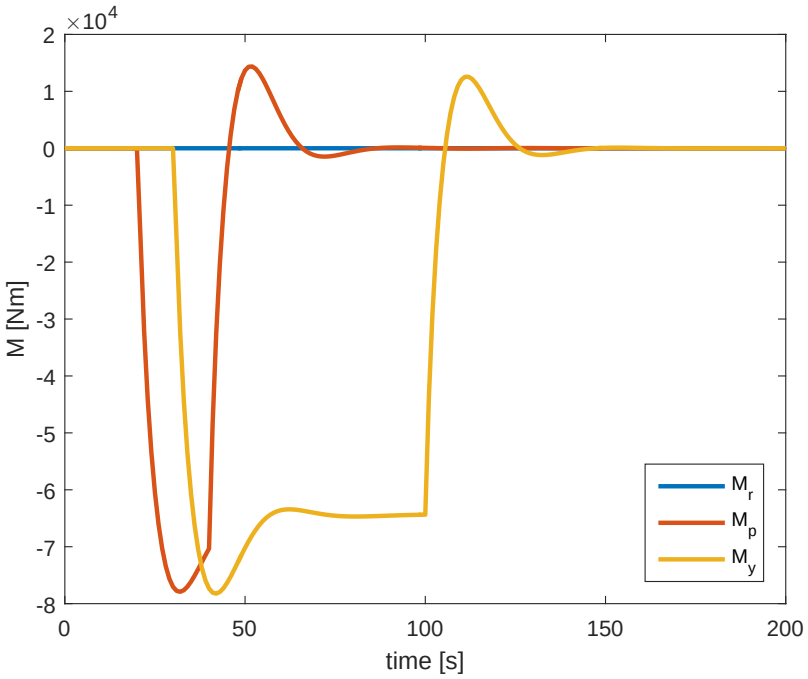

Figure 4.7: Aerodynamic moments acting on the launch vehicle over time

4.4 Linear Model

Nonlinear mathematical model has been developed in the previous section and serves as a good source of equations for the computer simulation. In order to assess the dynamics of the rigid body launch vehicle, a linear state-space model is introduced here in the form of

$$\dot{x} = Ax + Bu \tag{4.1}$$
$$y = Cx + Du \tag{4.2}$$

The state variables, inputs and outputs of our linear system are defined as

$$x = \begin{bmatrix} \dot{x} & \dot{y} & \dot{z} & x & y & z & p & q & r & q_0 & q_1 & q_2 & q_3 \end{bmatrix} \tag{4.3}$$
$$u = \begin{bmatrix} \delta_\theta & \delta_\psi \end{bmatrix} \tag{4.4}$$
$$y = x \tag{4.5}$$

The nonlinear model has been linearized with the help of MATLAB's `linmod` function for velocity of 600 m/s. The state-space matrices are truly extensive so they are presented here only in their substituted versions. It can already be stated that matrix C is an identity matrix and D is a zero matrix. The 0.0 values represent numbers of a small order but still not equal to zero.

$$A = \begin{bmatrix} 0.0 & 0 & 0.0 & -0.0 & 0 & 0.0 & 0 & 0 & 0 & -19.63 & 0 & 0 & 0 \\ 0 & 0 & 0 & 0 & 0.0 & 0 & 0 & 0 & 0 & 0 & 0 & 0 & -19.63 \\ 0 & 0 & -0.46 & 0.0 & 0 & -0.0 & 0 & 0 & 0 & 0 & 0 & 19.63 & 0 \\ 1 & 0 & 0 & 0 & 0 & 0 & 0 & 0 & 0 & 0 & 0 & 0 & 0 \\ 0 & 1 & 0 & 0 & 0 & 0 & 0 & 0 & 0 & 0 & 0 & 0 & 0 \\ 0 & 0 & 1 & 0 & 0 & 0 & 0 & 0 & 0 & 0 & 0 & 0 & 0 \\ 0 & 0 & 0 & 0 & 0 & 0 & -65.32 & 0 & 0 & 0 & 0 & 0 & 0 \\ 0 & 0 & -0.01 & 0 & 0 & 0 & 0 & -0.37 & 0 & 0 & 0 & 0 & 0 \\ 0 & 0 & 0 & 0 & 0 & 0 & 0 & 0 & -0.37 & 0 & 0 & 0 & 0 \\ 0 & 0 & 0 & 0 & 0 & 0 & 0 & 0 & 0 & 0 & 0 & 0 & 0 \\ 0 & 0 & 0 & 0 & 0 & 0 & 0.5 & 0 & 0 & 0 & 0 & 0 & 0 \\ 0 & 0 & 0 & 0 & 0 & 0 & 0 & 0.5 & 0 & 0 & 0 & 0 & 0 \\ 0 & 0 & 0 & 0 & 0 & 0 & 0 & 0 & 0.5 & 0 & 0 & 0 & 0 \end{bmatrix} \tag{4.6}$$

$$B = \begin{bmatrix} 0 & 0 \\ 10.88 & 0 \\ 0 & 10.88 \\ 0 & 0 \\ 0 & 0 \\ 0 & 0 \\ 0 & 0 \\ 0 & 6.19 \\ -6.19 & 0 \\ 0 & 0 \\ 0 & 0 \\ 0 & 0 \\ 0 & 0 \end{bmatrix} \tag{4.7}$$

If we compare the nonlinear model with the linear one, the results are consistent. With a short one second thrust vectoring impulse for δ_θ, the responses are almost identical as demonstrated in figures 4.8 and 4.9.

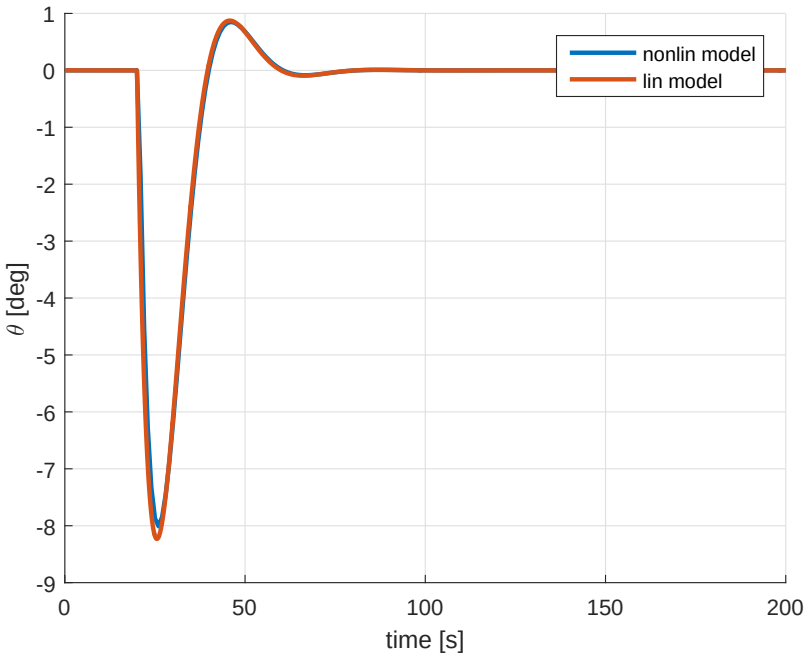

Figure 4.8: Nonlinear and linear model pitch angle θ responses comparison

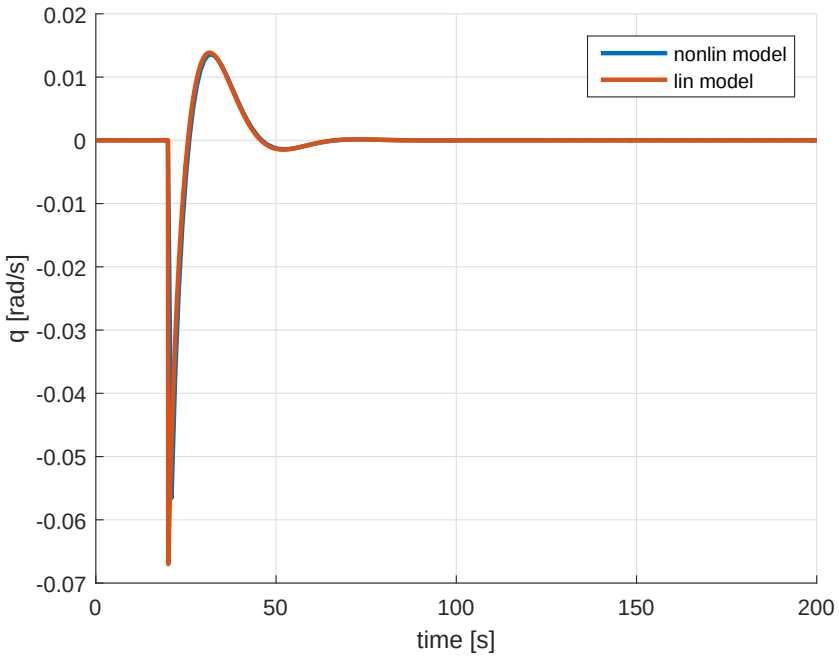

Figure 4.9: Nonlinear and linear model angular velocity q responses comparison

The linear model may serve as an initial source for launch vehicle's control laws analysis and regulators design.

4.4.1 Sensitivity Analysis

As stated above, the vehicle's dynamics highly vary with velocity and other parameters. In order to qualify such relations, a basic sensitivity analysis has been conducted.

The distribution of poles resembles an airplane's dynamics with one real stable poles, one oscillatory mode and one integrator [15]. Three separate quantities have been analyzed. At first, the launch vehicle system has been linearized with respect to changing velocity. Note the pair of complex conjugate poles causing oscillations during the launch vehicle's flight. They are caused by aerodynamic forces and moments returning the spacecraft into vertical position after any intended or random disturbance. A slight tendency of the poles to become more stable as the vehicle speeds up can be observed in figure 4.10. Moreover, from a certain boundary velocity, the oscillations of complex conjugate pair of poles is slowing down. Note that the aerodynamic coefficients were set to the same constant values for all velocities. Real stable poles at -75, -20, -5 and -1 are omitted in the figure 4.10.

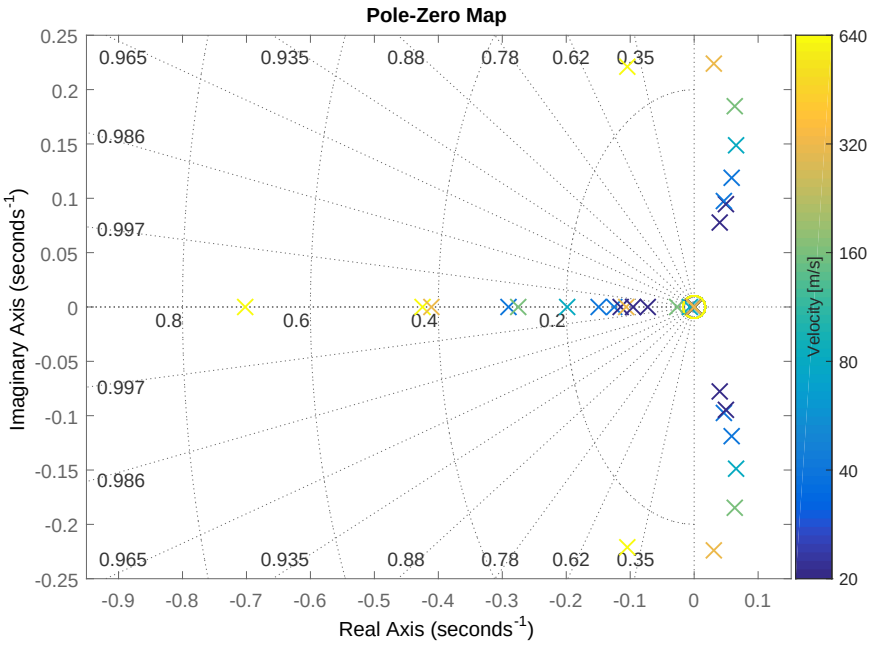

Figure 4.10: Poles and zeros of the system in relation to velocity

The figure 4.11 represents the linearization with respect to the main moments of inertia with constant vehicle's velocity set to 400 m/s. Although only the J_{11} moment is displayed in the legend, another two main moments J_{22} and J_{33} have been varied proportionally. It is observed that as the value of the moments rises, the complex poles' oscillation velocity slackens and the poles become more stable which corresponds to common sense. The higher the moment of inertia is, the harder to accelerate the object is. The moment's value used throughout the simulations is in the middle of the legend range. Real stable poles at -430, -220, -110, -50 and -25 are omitted in the figure 4.11.

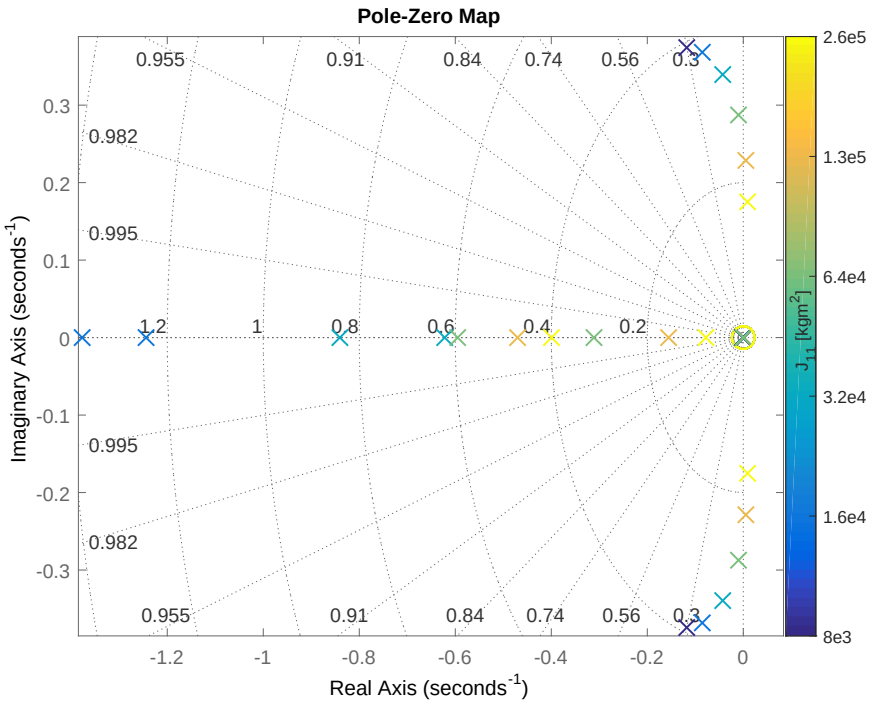

Figure 4.11: Poles and zeros of the system in relation to moment of inertia

The plot 4.12 shows the relation between launch vehicle's poles and the pitch moment aerodynamic coefficient for angle of attack with constant vehicle's velocity set to 400 m/s. As the coefficient's value rises the rate of system's oscillations increases and its poles move to the edge of stability. That has been validated by the simulation model. The value of C_{Mp_α} used in the simulations is usually set to 0.05. Real stable poles at -14 is omitted in the figure 4.12.

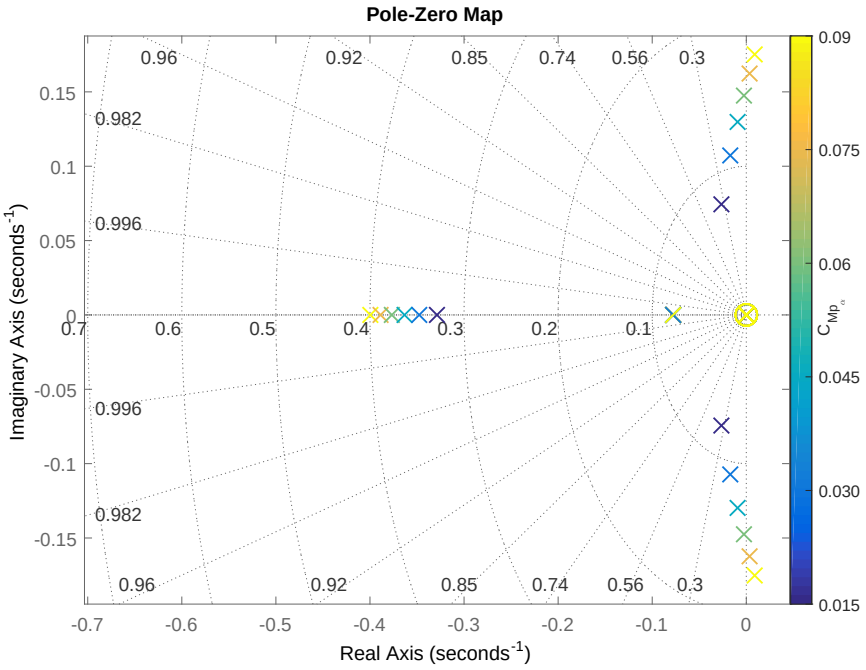

Figure 4.12: Poles and zeros of the system in relation to pitch moment coefficient for α

4.5 GUI

One of the ideas behind building a functional launch vehicle flight simulation model has been the intention to present a simple visualizations to students interested in aerospace field. Thus a MATLAB GUI has been designed as a part of the thesis.

The GUI is decomposed into three tabs. The first tab in figure 4.13 contains launch vehicle's trajectory visualization with ground trace of the trajectory. Next, a simple 3D rocket model is used to demonstrate the YPR angles. The 3D graphics has been downloaded from www.thingiverse.com under the name "Classic Rocket" created by user called "Botmaster" [16]. Visualizations are accompanied by launch vehicle's current position, velocity and values of its YPR angles.

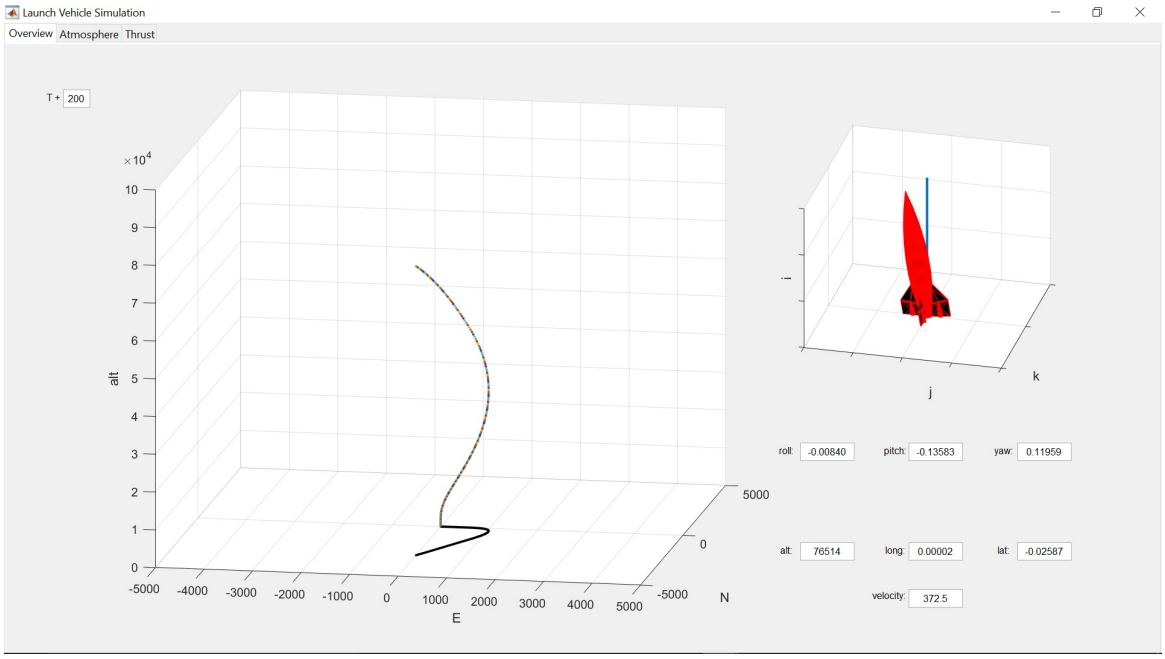

Figure 4.13: Launch Vehicle Simulation MATLAB GUI - first tab

In the second tab in figure 4.14 a set of life updating atmospheric data is presented. Plots of altitude over time and ambient pressure, temperature or air density over altitude can be found there.

The third tab visible in figure 4.15 bellow represents the thrust over time updating plot.

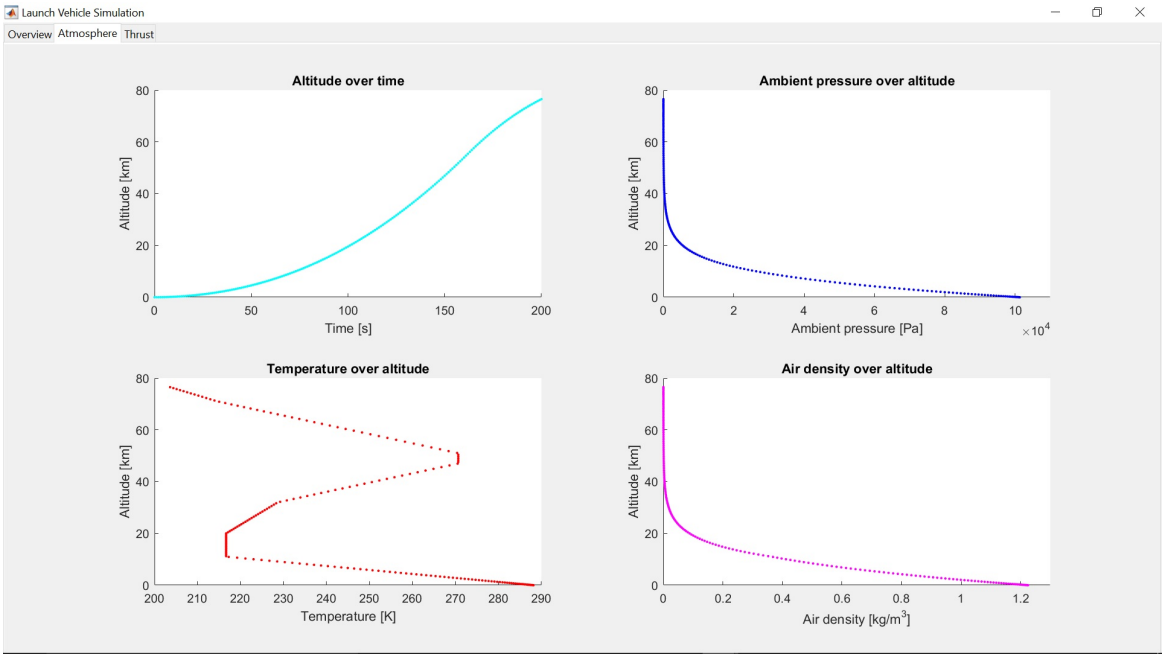

Figure 4.14: Launch Vehicle Simulation MATLAB GUI - second tab

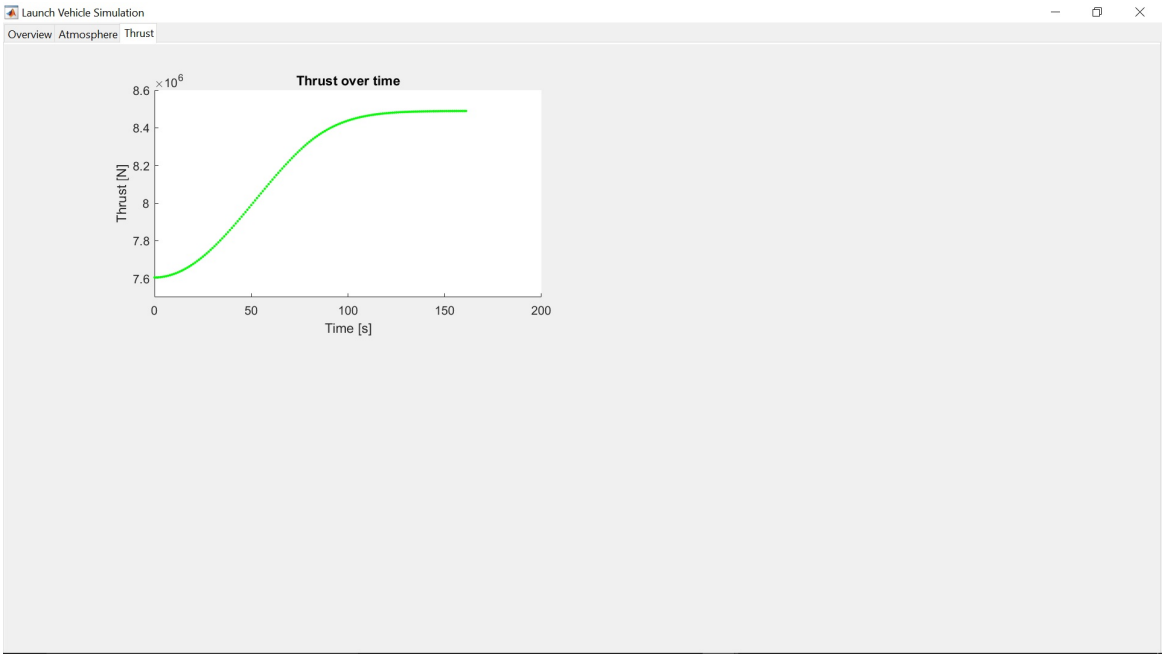

Figure 4.15: Launch Vehicle Simulation MATLAB GUI - third tab

Chapter 5

Water Rocket Experiment

The aim of a practical experiment is to demonstrate how well mathematical model reflects reality. We will join an already established team from the Faculty of Electrical Engineering at the Czech Technical University under the guidance of *Ing. Petr Kočárník, Ph.D.* Their objectives are very extraordinary indeed. With a couple of colleagues they have developed a launch vehicle reactive water model ELEKTRON I.

As stated in their informational leaflet [17], ELEKTRON I is designed as plastic rocket with propulsion provided by water and pressurized air due to safety reasons. The head of the model is equipped with parachute and ejection mechanism for safe landing. Nose cone encapsulates flight sensors (accelerometer and magnetometer) and control unit.

Although our simulation model has been designed for real world big launch vehicles, any experiments with those are beyond our capabilities. The accessible water rocket model has to be sufficient. The original idea was to simulate a flight of ELEKTRON I in the Simulink environment with set tilt sequence of control fins. Likewise, the real ELEKTRON I would be launched with the identical preprogrammed control fins tilt sequence and flight data including trajectory, velocity and acceleration would be collected. When performed several times, enough data for the accuracy assessment of our simulation model and its possible calibration should be obtained.

Unfortunately, due to uninfluencable circumstances, we were unable to carry out the described experiment in time. Nevertheless, data from former model's uncontrolled flight has been acquired. Those data are used to calibrate the simulation model for the water rocket model, to estimate unknown quantities and prepare it for further employment.

5.1 Input data

All available quantities defining the water rocket model are summarized in the table 5.1 below.

Quantity	Symbol	Value
Mass without water	m_{empty}	1134 g
Length	l	2080 mm
Diameter	d	110 mm
Tank volume	V_{tank}	12.6 l
Initial water volume	V_{water_i}	$2,7$ l
Initial air pressure	p_{air_i}	10 bar
Aerodynamic reference area	S	8171 mm^2
Drag coefficient	C_D	0.4
MAX achieved altitude	h_{max}	170 m
MAX achieved velocity	v_{max}	45 ms^{-1}
MAX achieved acceleration	a_{max}	38 ms^{-1}
Main moments of inertia	J_{11}, J_{22}, J_{33}	10^9, 10^6, 10^9 gmm^2

Table 5.1: Water rocket model input data

Other data necessary for the simulation had to be estimated. The water rocket's thrust has been modeled with a simplified version of equation 3.69 where only the difference between exit and ambient pressures is considered. The only known aerodynamic coefficient is the drag coefficient and the estimation of others cannot be verified due to lack of experimental data. The estimated constants are summarized in the table 5.2 below.

Quantity	Symbol	Value
Exit pressure	p_e	1×10^6 Pa
Nozzle exit area	A_e	3.3×10^{-5} m
"Burn" time	t_{burn}	3 s
Axial force coefficient	C_A	0.4
Axial force coefficient for α	C_{A_α}	0.1
Axial force coefficient for β	C_{A_β}	0.1
Side force coefficient for β	C_{S_β}	0.2
Normal force coefficient for α	C_{N_α}	0.2
Roll moment coefficient for p	C_{Mr_p}	0.3
Pitch moment coefficient for α	C_{Mp_α}	0.01
Pitch moment coefficient for q	C_{Mp_q}	0.3
Yaw moment coefficient for β	C_{My_β}	0.01
Yaw moment coefficient for r	C_{My_r}	0.3

Table 5.2: Estimated water rocket model input data

5.2 Outcomes

The real flight data are compared to the calibrated Simulink model outcomes in the plots below. A software issue has arisen during the test flight causing the accelerometer on board of the water rocket to start measuring only after the first second of flight which can be seen in all the following figures from 5.1 to 5.3.

With slight tuning of the initializing engine defining constants, the developed simulation model projects the rocket's altitude very accurately as can be seen in figure 5.1 below. While the thesis is focused only on the lift-off phase of the flight, model's descent is not covered.

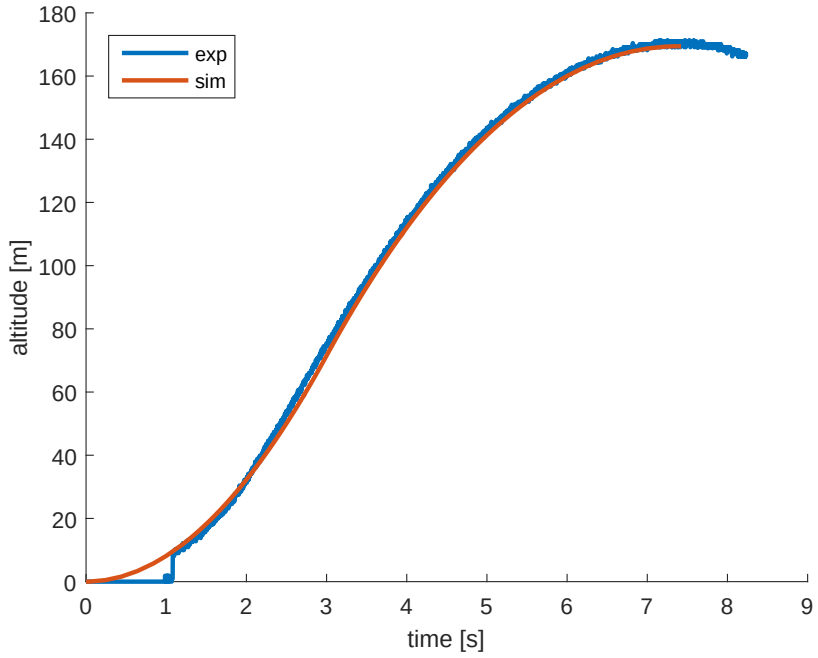

Figure 5.1: Water rocket experimental and simulation altitude results comparison

The biggest source of disturbances for the light water rocket model are definitely wind gusts. While the simulation model does not include any wind submodel, the rocket's deflections cannot be satisfactorily modeled. However, at least a rough match has been found between the experimental and simulation results for the vertical acceleration visible in figure 5.2 on the next page.

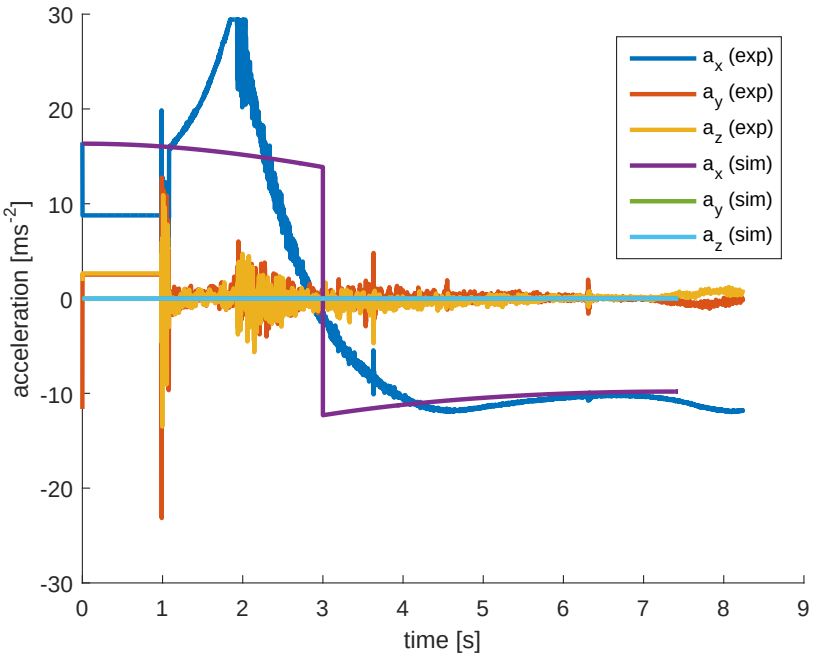

Figure 5.2: Water rocket experimental and simulation acceleration results comparison

The mass of the water rocket model may not be equally spread causing the rocket to tilt to one side. That is probably the case here while the angular velocity especially about the z axis recedes from zero immediately after launch. Another source of disturbances is the already mentioned wind. Due to these reasons, the experimental results could not have been matched with the simulation outcomes. So only the experimental flight data are presented in figures 5.3 bellow.

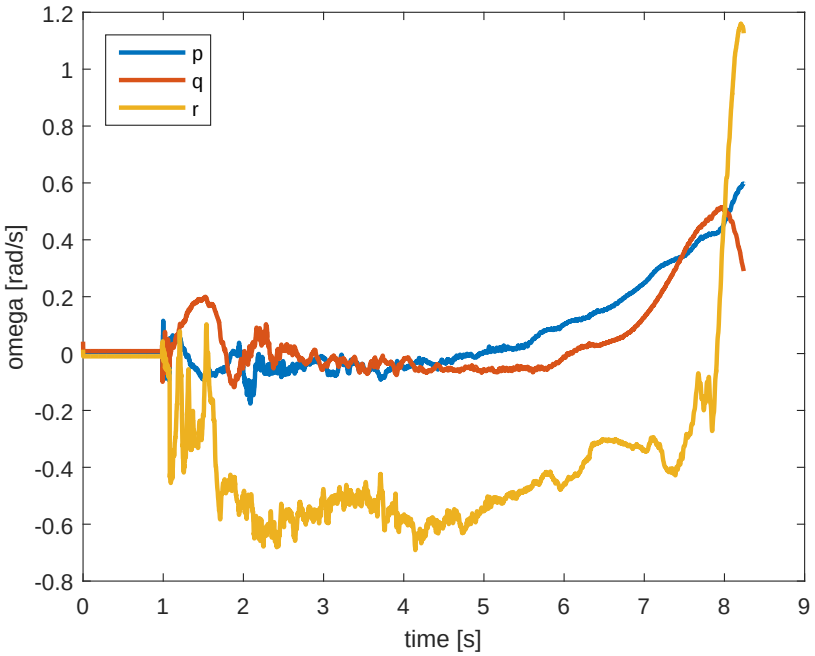

Figure 5.3: Water rocket experimental angular velocity results

Data from the onboard magnetometer are not presented here while it holds no significance for the developed simulation model.

Chapter 6

Results

Let's recapitulate what have been accomplished by this thesis and summarize the results.

Reference frames. Several reference frames have been partially adopted from literature in order to maintain conformity with general conventions in aerospace industry. Some, such as the Earth geographic frame, were on the other hand newly defined with the hope of better meeting the project's specifications. Individual transformation rotational matrices were described and more complex transformations between frames can be built upon them.

Rotational kinematics. The rotational kinematics serves as a basis for further modeling and simulation while it provides us with launch vehicle's attitude in space determination in terms of yaw, pitch and roll angles. Highly flexible quaternions with the advantage of no dangerous singularities and shorter computation time have been utilized instead of not so suitable but easily imaginable Euler angles. Necessary relations between both forms are provided.

Dynamics. Drawing from the Newton's and Euler's laws, translational and rotational dynamic models have been developed with not fully specified forces and moments. Those are described in detail in sections about the Earth gravitational field, atmosphere and aerodynamics and rocket propulsion and control. Several important assumptions have been made along the way with the aim to keep the model's description clear but still precise enough.

Equations of motion. When combined together, set of thirteen equations of motion surfaced. Those equations have been implemented in the MATLAB and Simulink simulation of launch vehicle's flight. The model has been built with the thought of future expansion and each subsystem can be easily altered for different utilization. Numerical values soon became necessary for model validation. Some were obtained from published real launch vehicles' specifications, others had to be estimated and manually tuned. Probably the greatest challenge of our simulation model is the partial uncertainty of the numerical quantities. As we have learned along the way, each value can radically alter the simulation results.

Simulation. After the theoretical equations have been adjusted optimally for our model, the Simulink model tuning could have begun. The process was demanding due to the absence of complete set of launch vehicle defining numerical values. Meaningful model results have been given priority to accurate constants. The model has been verified by multiple test flights. Each of them with different set of thrust vectoring or fins control commands, distinct initial values, and situations. We focused on comparing the present launch vehicle's behavior to

theoretical assumptions. For example, it is clearly visible from the figures 4.6 and 4.7 how the aerodynamic moments are returning rocket to its initial vertical position. The forces and moments are actually acting as dampers on spring and the coefficients can be assimilated to spring constants which is in agreement with the theory. The modeled flight data are depicted by the user friendly, life updating GUI for further accessibility.

Stability. The constant aerodynamic coefficients also represent probably the biggest drawback of our approach as they vary a lot with respect to vehicle's velocity in reality. The aerodynamic forces and moments are likewise affected by the position of the center of pressure and concept called the *stability margin*. While the position of c.p. has to be determined experimentally or using Computational Fluid Dynamics methods, stability margin is a distance between c.g. and c.p. and tells us how stable the aircraft actually is. While we see some instability in figure 4.10, the "constantness" of aerodynamic coefficients could be a reason. In other words, the rocket should be stable for all velocities with the right set of aerodynamic coefficients.

Water rocket. Although the initially designed practical experiment could not have been executed, a set of already obtained flight data has been compared to the simulation model outcomes. Wherever possible, the estimated constants have been verified with respect to the real results and may serve as a basis for further water rocket aerodynamics assessment. What had been seen as the greatest challenge, to readjust the simulation model intended for big launch vehicles to small rocket models, actually appeared viable as can be stated for example based on figure 5.1. However, both outer and inner dynamics of a water rocket are different from a launch vehicle's. Should the water rocket be simulated more profoundly, specialized Simulink subsystem models may be developed and greater set of flight data collected.

Chapter 7

Conclusion

Numerous voluminous books and studies have been written about rocketry and launch vehicles flight laws. It is not possible to cover the problematics in its whole width and depth in a single thesis. However, satisfactory mathematical model has been developed and platform for simulating rocket flight described throughout this work.

In sum, all goals initially set in chapter 2 have been fulfilled. The equations describing rocket motion have been developed and utilized in the simulation model development. The Simulink model has been verified and tested in multiple situations, then. A simple yet informative GUI has been introduced to visualize the simulation results in time. Beyond the thesis' guidelines, the original nonlinear model has been linearized and a basic sensitivity analysis has been performed. In the end, a practical experiment has been documented and our model calibrated with respect to the flight data results.

There is a plenty of space for future research. The Simulink model could be validated by broader set of experimental water rocket flights with fins control involved. The linearized model may serve as a basis for control laws development and automatic regulators design. Further research may look into the rocket's aerodynamics in hypersonic velocities and experimentally determine the values of aerodynamic coefficients. As has been already stated, the simulation model is highly expandable and versatile. More precise subsystems can be implemented, multiple stage or flexible body rockets introduced. The developed simulation model can serve as a platform for various cases.

How else to round off a rocketry thesis than by an apt phrase "Per aspera ad astra"!

Appendix A

Contents of the attached CD

- `rocketsim.slx` - Simulink model
- `init.m` - initialization of simulation
- `analyze.m` - analysis of simulation results
- `gui.m` - visualization of simulation results, GUI
- `tiltFin.m` - fins control used by `rocketsim.slx`
- `rotX.m`, `rotY.m`, `rotZ.m` - rotation matrices used by `rocketsim.slx`
- `omegaJ.m` - part of Euler equations used by `rocketsim.slx`
- `ECF2EG.m` - transformation from ECF to EG frame used by `rocketsim.slx`
- `rocket.stl` - rocket 3D model used for visualization by `gui.m`
- `README.txt` - readme file, instruction manual for the simulation

Bibliography

[1] Peter H. Zipfel. *Modeling and Simulation of Aerospace Vehicle Dynamics*. 2nd. AIAA, 2007. ISBN: 9781563478758.

[2] International Earth Rotation and Reference System Service. *Bulletin B 344*. 1.10.2016.

[3] Bong Wie. *Space Vehicle Dynamics and Control*. 2nd. AIAA, 2008. ISBN: 9781563479533.

[4] James Diebel. "Representing attitude: Euler angles, unit quaternions, and rotation vectors". In: *Matrix* 58 (2006).

[5] Wei Du. *Dynamic modeling and ascent flight control of Ares-I Crew Launch Vehicle*. Iowa State University, 2010.

[6] National Imagery and Mapping Agency. *World Geodetic System 1984*. 3rd. NIMA, 3.1.2000.

[7] Robert F. Stengel. *Flight Dynamics*. Princeton University Press, 2004. ISBN: 0691114072.

[8] National Oceanic Atmospheric Administration, Department of the Air Force, and NASA. *U.S. Standard Atmosphere, 1976*. 1976.

[9] *The Beginner's Guide to Aeronautics*. URL: https://www.grc.nasa.gov/WWW/K-12/airplane/ac.html (visited on 09/04/2017).

[10] Filip Svoboda. *Research report: Water rocket project*. Czech Technical University, 2015.

[11] Warrick Miller. *Lecture notes: Space Vehicle Design (MECH ENG 3104)*. The University of Adelaide, 2016.

[12] Space Exploration Technologies Corp. *Falcon 9 Launch Vehicle Payload User's Guide, Rev 2*. SpaceX, 2015.

[13] *Falcon 9 FT*. URL: http://spaceflight101.com/spacerockets/falcon-9-ft/ (visited on 09/04/2017).

[14] *Saturn V Launch Simulation*. URL: http://www.braeunig.us/apollo/saturnV.htm (visited on 09/04/2017).

[15] Martin Hromcik. *Presentation slides: Flight dynamics*. Czech Technical University, 2013.

[16] *Classic Rocket by Botmaster*. URL: http://www.thingiverse.com/thing:580192 (visited on 10/04/2017).

[17] Petr Kocarnik. *Information leaflet: ELEKTRON I*. Czech Technical University, 2015.